Advances in Colloid and Interface Science 358 (2026) 104066

Contents lists available at ScienceDirect

Advances in Colloid and Interface Science

journal homepage: www.elsevier.com/locate/cis

The Interface Science Data Repository: A (meta)data framework and platform for FAIR data reporting in experimental fluid interface science

Pascal Bertsch [a,b,*], Emmanouil Chatzigiannakis [c,d], Peter Fischer [e], Emma Hinderink [f], Lucio Isa [g], Martin Leser [a], Julia Maldonado-Valderrama [h], Reinhard Miller [i], Brent S. Murray [j], William E. Robinson [k], Leonard Sagis [l], Jacopo Vialetto [m,n], Jack Yang [l], Martin Malmsten [o,p]

[a] Department of Chemistry, University of Fribourg, Switzerland
[b] Food Research and Innovation Center, University of Fribourg, Switzerland
[c] Processing and Performance Group, Mechanical Engineering Department, Eindhoven University of Technology, the Netherlands
[d] Institute of Complex Molecular Systems, Eindhoven University of Technology, the Netherlands
[e] Institute of Food Nutrition and Health, ETH, Zurich, Switzerland
[f] Multiphase Systems (ME-P&E), Delft University of Technology, the Netherlands
[g] Laboratory for Soft Materials and Interfaces, ETH Zurich, Switzerland
[h] Department of Applied Physics, University of Granada, Spain
[i] Institute for Condensed Matter Physics, Technical University Darmstadt, Germany
[j] Food Colloids and Bioprocessing Group, School of Food Science and Nutrition, University of Leeds, UK
[k] Department of Physical Organic Chemistry, Institute for Molecules and Materials (IMM), Radboud University, the Netherlands
[l] Laboratory of Physics and Physical Chemistry of Foods, Wageningen University, the Netherlands
[m] Department of Chemistry "Ugo Schiff", University of Florence, Italy
[n] Consorzio per lo Sviluppo dei Sistemi a Grande Interfase (CSGI), Italy
[o] Department of Chemistry, Lund University, Sweden
[p] Department of Pharmacy, University of Copenhagen, Denmark

ARTICLE INFO

Keywords:
Tensiometry
Interfacial rheology
Surface-active species
Database
Machine learning
Neural network models

ABSTRACT

Interface science, i.e., the study of adsorption, phase behavior and flow of matter at liquid interfaces, is a highly interdisciplinary research area that brings together researchers from fundamental theory to industrial production. FAIR – Findable, Accessible, Interoperable, Reusable – reporting of data and metadata is currently not common practice in interface science, although it could considerably promote the reuse of data across disciplines and foster translations to industry. For research fields with heterogeneous, non-standardized datasets such as interface science, community-driven agreement on relevant data, metadata, and reporting formats is an essential prerequisite before more advanced machine-operable infrastructures can be developed. We here propose a framework for relevant data and metadata for different interface science methods, surface-active species, and liquid subphases. We further introduce the Interface Science Data Repository (zenodo.org/communities/isdr) to provide a common platform for sharing interface science data. We discuss considerations for future machine-operable interface science databases and how standardized reporting can facilitate the development of data-driven modelling approaches, including machine learning. We hope that this work represents a first step towards establishing an active culture of FAIR data sharing in interface science while laying the groundwork for increasingly interoperable and automated data infrastructures.

1. Introduction

Interface science is the study of physical and chemical phenomena that occur at liquid-liquid and liquid-gas interfaces. Such interfaces are ubiquitous in nature and many industrial applications; they play a vital role in physiology and medicine [1–7], biology [8–11], oceanography

* Corresponding author at: Department of Chemistry, University of Fribourg, Switzerland.
E-mail address: pascal.bertsch@unifr.ch (P. Bertsch).

https://doi.org/10.1016/j.cis.2026.104066
Received in revised form 28 July 2026;
Available online 5 October 2026
0001-8686/© 2026 The Authors. Published by Elsevier B.V. This is an open access article under the CC BY license (http://creativecommons.org/licenses/by/4.0/).

[12–14], as well as in drug delivery [15–17], cosmetics [18,19], foods [20–23], and materials science [24,25]. Consequently, interface science is a melting pot for researchers from diverse backgrounds and industries. These areas all have different focuses, and the role of fluid interfaces varies in each discipline. In some areas, they are the main scope of research, while in others they may merely be a secondary boundary condition. This leads to different cultures and traditions in the investigation of these systems and communication of results, pointing to a need for data standardization and the establishment of an internationally accepted baseline for data reporting. Despite the diversity of fluid interfaces and involved disciplines, the phenomena studied are often closely related. Most interface science studies investigate the behavior of surface-active species and other materials that assemble at fluid interfaces, i.e., their adsorption, interfacial structure, and rheology. The potential overlap of interface science studies is eminent, and it is likely that findings from one discipline could be of considerable value also in another field or industry. For example, the protein lysozyme found in animals is a prominent model protein used to study the adsorption of proteins in experiments [26] and simulations [27], whilst it is an inherent constituent of the eye tear film [28], an important foaming agent in egg white foam [29], or can be used for the assembly of antimicrobial 2D coatings [25] (Fig. 1). However, there is currently no active culture of data sharing in interface science, a consensus on data standards, nor a common platform for data sharing. Interestingly, interface science does have an active culture of data reuse. There are several examples of studies that reused previous data to extend their datasets or to draw new conclusions in a different context, for example for proteins [30–33], surfactants [34–44], particles [45], or mixed interfacial layers [46–48]. Robinson and colleagues [49] established an extensive database for surfactant adsorption data, SurfPro, alongside a graph neural network model that can predict surfactant adsorption based on surfactant structure, which was recently updated to a relational database with data curation workflow [50]. As a practical example, several databases and related neural networks were established to link the structure of surfactants or their foams to their fire-extinguishing performance [51–54]. These cases demonstrate the potential of data reuse in interface science, but also stress the need for clear guidelines and a common platform to share interface science data and facilitate reuse.

There is an overall trend towards open science practices, partly pushed by funding agencies and publishers, but also supported by an increased acceptance and willingness of researchers [55]. Today, the majority of researchers is willing to share and reuse data, and agree that limited data access is ‘a major impediment to progress in science at large’. [56] A recent cross-disciplinary survey found that combining multiple previous datasets to answer new research questions is the most common purpose for data reuse, but also pointed out that researchers often struggle to find relevant datasets [57]. The open sharing of data is correlated with higher citation rates [58–60], demonstrating the increased reuse and transferability of studies that make their data available. Last but not least, the emergence of machine learning makes research data a veritable treasure for the training of neural networks and predictive models [61,62]. However, any (meta)data not shared appropriately must be considered lost, or at best incomplete, for any future use.

We anticipate that there lies great potential in the reuse of interface science data. An important requirement to fully harness this potential is the meticulous sharing of data and metadata following open science standards, e.g., according to FAIR-principles [63–65]. The FAIR principles aim at exploiting the full potential of scientific data by making it Findable, Accessible, Interoperable, and Reusable for other researchers and machines. The key guiding principles are to make data and supplementing metadata:

- *Findable,* for instance, by depositing data along with rich metadata in a trusted and indexed repository that assigns a persistent identifier (e.g., DOI).

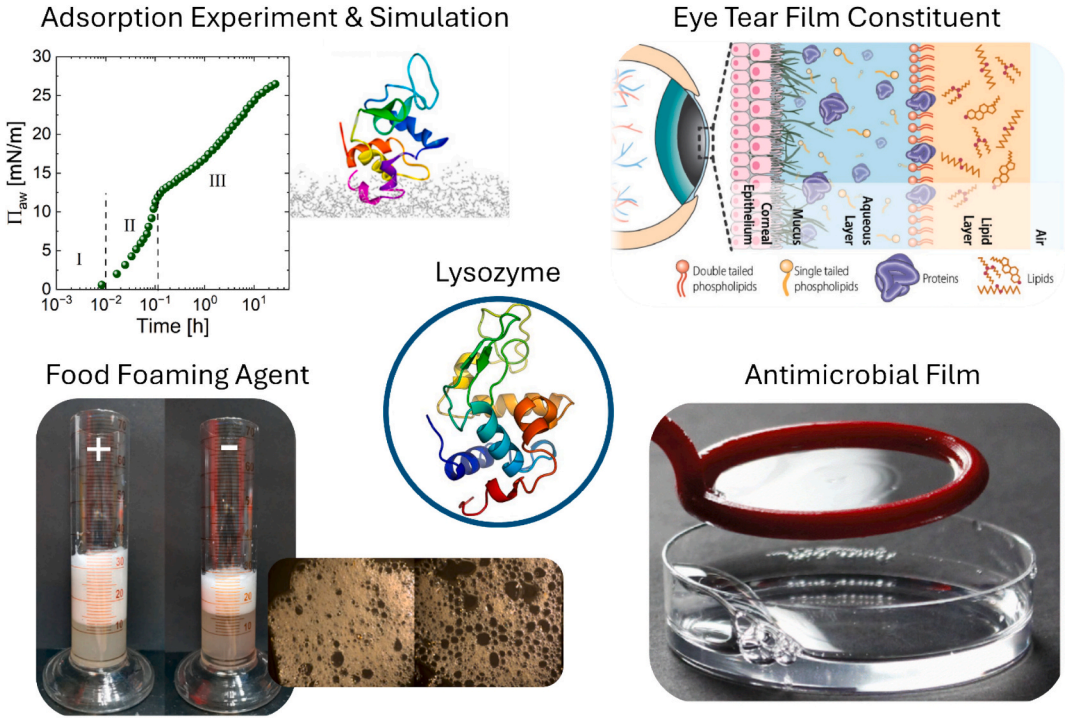


Fig. 1. Example showcasing the potential transferability of interface science data: The protein lysozyme is an extensively investigated model protein used in adsorption experiments and simulations. It is also an inherent constituent of the human eye tear film, plays an important role in egg white foam, and displays antimicrobial properties which can be harnessed to create 2D antimicrobial films and coatings. Reproduced with permission from Freer et al. (Ref. 26, Arooj et al. (simulation, Ref. 27, Bertsch et al. (tear film schematic, Ref. 28, Zhao et al. (egg white foam, Ref. 29, and Kummer et al. (2D film, Ref. 25.

- *Accessible,* by making data as openly accessible as possible, providing authentication and authorization procedures if necessary, and using standardized communication protocols for machine-actionability.
- *Interoperable,* by using standard and commonly applicable file formats, language, and vocabulary, and including qualified references to other (meta)data.
- *Reusable,* by providing richly described (meta)data with detailed provenance that meets discipline specific standards under a Creative Common license.

The FAIR principles have been postulated as universal guidelines for scientific data and must therefore be adapted and reinterpreted for specific scientific disciplines [66,67]. In some disciplines, it is common practice to deposit (meta)data in highly specialized repositories with detailed guidelines for dataset structure and formats. Popular examples include the GenBank [68], the Protein Data Bank [69], and the SIMBAD database for astronomical objects [70]. Of course, such unified standards greatly facilitate the interoperability and reusability of deposited (meta)data, particularly by machines. Many scientific disciplines, including interface science, are not structured around such universally standardized data**.** **T**his lack of standards for data reporting makes it hard to guarantee that (meta)data is sufficiently FAIR. Recent efforts to collect and curate interface science data for surfactants [49] (zenodo.org/records/14931937) and proteins [32] (zenodo.org/records/18799688) exemplify the challenges encountered. In both cases, authors reported hurdles to find and extract data in suitable form or missing (meta)data. An important step towards ensuring data quality is thus for communities to self-organize and define standards for FAIR (meta)data sharing in their scientific sub-fields [66], as recently seen in related research areas, particularly materials chemistry [71–74]. We here aim to provide such a framework for FAIR (meta)data sharing in experimental interface science, by defining what (meta)data reporting is required for typical fluid interface science experiments, surface-active species, and liquid subphases. We further establish an initial human-operated data repository for the sharing of interface science data. We hope that the presented guidelines and data repository provide a first step towards a vivid culture of data sharing and reuse, as well as triggering further discussions in the community on how to shape the future of data sharing in fluid interface science.

2. Interface science data and metadata framework

The aim of the current framework is to define the data and metadata required for facile and meaningful reuse of fluid interface science data. We refer to *Data* as the values obtained in typical interface science experiments, e.g., the interfacial tension as a function of time upon adsorption of a surface-active species at interface. *Metadata* corresponds to all extra information that puts this data in a meaningful context, i.e., all relevant information about the surface-active species, subphases, and environmental conditions, as well as detailed information regarding the methodology used.

2.1. Data and methodology

2.1.1. Surface and interfacial tension measurements

Tensiometry aims at measuring the air-water surface tension γ_{aw} or oil-water interfacial tension γ_{ow}, often in presence of surface-active species that reduce γ. Key parameters of interest include the adsorption kinetics, i.e., the reduction of interfacial tension versus adsorption time $\gamma(t)$, or the equilibrium interfacial tension γ_{eq} of surface-active species depending on their bulk concentration. Some species show an induction time before adsorption during which the interfacial tension remains close to that of the clean interface [75]. Furthermore, while small molecular weight surfactants may reach γ_{eq} within seconds [41], other materials like globular proteins [31] or hydrophilic nanoparticles [76] may take 24 h or longer to reach (quasi-)stable γ. It is thus important to report the criteria used to determine the formation of a stable interfacial layer.

Reporting of γ_{eq} as a function of concentration of the surface-active species is useful to extract additional information from adsorption isotherm models [77], such as the surface excess Γ or critical micelle concentration (CMC) of surfactants via the Gibbs adsorption isotherm [41,78] or the adsorption energy E_{ad} of micro- or nanoparticles via a displacement approach [79], as discussed in detail below. A control measurement of γ_0 for at least a few minutes, or ideally equivalent to performed experiments, is critical to confirm the absence of surface-active contaminants. The obtained γ_0 further acts as a control that the measuring setup is properly adjusted and should be ≈ 72.4 mN/m for γ_{aw} at room temperature or close to literature values for γ_{ow} [80,81]. Reporting of γ_0 allows calculation of the interfacial pressure $\Pi(t) = \gamma_0 - \gamma(t)$ or normalized interfacial pressure $\pi(t) = \Pi(t)/\gamma_0 = (\gamma_0 - \gamma(t))/\gamma_0$. For tensiometry techniques relying on drop or bubble shape, reporting the Bond number Bo describing the balance of gravitational forces and γ is critical to comprehend reported data [82,83]:

$$\mathrm{Bo} = \frac{\Delta\rho g R^2}{\gamma}$$

where $\Delta\rho$ is the density difference between the two phases, g is the gravitational force and R is the droplet radius. Bo should be in the range of 0.1-1 to provide a balance of gravitational elongation and shape-retaining γ. Berry et al. [82] recently extended this concept and introduced the Worthington number Wo accounting for needle radius. Ideally, relevant drop images are provided to allow refitting of the drop shape. For the Wilhelmy-plate technique, raw force data alongside the plate and trough material and circumference will allow to reenact interfacial tension calculations [84,85]. An overview of relevant data for interfacial tension measurements is provided in Table 1.

2.1.2. Interfacial compression and dilatational rheology experiments

Some tensiometry setups**,** such as the pendant drop or Langmuir–Blodgett troughs further facilitate the modulation of the surface area A by altering the drop volume or movable barriers, respectively [89,90]. This allows generation of surface pressure-area Π-A isotherms to investigate 2D phase transitions or obtain the compressibility modulus E

Table 1
Overview of relevant data and metadata for interfacial tension measurements.

Data	Unit	Equation	Comment
Interfacial tension measurement data			
Interfacial tension change $\gamma(t)$	N/m	–	Ideally report raw data, i.e., bubble shape image plus subphase densities or force curves plus Wilhelmy-plate material and dimensions [82,86]
Induction time	s	–	–
Equilibrium interfacial tension γ_{eq}	N/m	–	Report at what time γ_{eq} was taken. For quasi-stable interfacial layers, report criteria to define the plateau value
Interfacial tension of clean interface γ_0	N/m	–	Important measure of subphase purity and oil polarity [80,81]
Method metadata			
Method	–	–	Report mode of measurement and instrument details [85,86]
Materials	–	–	Report material of used troughs, needles, or Wilhelmy-plate [84,85] Report radius of needles and circumference of Wilhelmy-plate
Surface area A	m^2	–	For Langmuir-Blodgett troughs, report shape and aspect ratio and Wilhelmy-plate positioning and orientation [87,88]
Bulk volume	m^3	–	Particularly relevant if adsorption occurs from a subphase
Bond number Bo	–	$Bo = \frac{\Delta\rho g R^2}{\gamma}$	For drop shape analysis methods [82,83]

of the interfacial film [91]:

$$E = -\frac{d\gamma}{dlnA}$$

Note that Π-A isotherms in both compression and expansion should be reported to detect hysteresis or relaxation effects. Step expansion-compression experiments can be valuable for complex interfaces that exhibit dynamic heterogeneity [92]. Periodic (sinusoidal, triangular) area oscillations applied to adsorbed interfacial layers allow determination of the interfacial dilatational storage modulus E' and loss modulus E". The interfacial area is oscillated around a mean area A_0 with a certain strain amplitude $\varepsilon = \Delta A/A_0$ and an oscillation frequency ω. E' and E" are defined as:

$$E' = \frac{d\gamma}{\varepsilon}cos\delta$$

$$E'' = \frac{d\gamma}{\varepsilon}sin\delta$$

where δ is the phase shift of γ in response to the area change. E' and E" typically vary as a function of ω as well as for ε beyond the linear viscoelastic regime. For comparability of E' and E" across different studies, it is therefore pivotal to unambiguously report ε and ω, or ideally, report E' and E" for several ε and ω to show their strain- and frequency-dependence. Full area oscillation-surface pressure cycles may be depicted in Lissajous plots to identify hysteresis and to extract further information on the (non-linear) behavior of interfacial layers under compression and extension, respectively [93,94]. For Langmuir-Blodgett trough experiments, the trough material and dimensions, as well as Wilhelmy plate material, positioning, and orientation relative to the compression should be reported as the uniaxial compression induces a superposed shear flow [87,88]. Many state-of-the-art pendant drop or Langmuir-Blodgett setups directly provide E' and E". The underlying oscillation cycles of γ and A or drop shape profiles are not routinely reported, although it might help researchers, reviewers, and others aiming to reproduce the data to understand contributions from anisotropic stresses [83,86] or superimposed adsorption phenomena [95,96] and support the development of new methods or numerical treatments [83,86]. An overview of relevant data for interfacial compression and dilatational rheology measurements is provided in Table 2.

Table 2
Overview of relevant data and metadata for Interfacial compression and dilatational rheology experiments. Method metadata corresponds to Table 1.

Data	Unit	Equation	Comment
Interfacial compression & dilatational rheology data			
Surface pressure -area isotherms Π(A)	N/m	–	Report interface formation procedure and equilibration time. Surface shape can be important due to superimposed shear flow [87,88]
Compressibility modulus E	N/m	$E = -\frac{d\gamma}{dlnA}$	Can depend on compression rate and aspect ratio [87,88]
Interfacial dilatational storage modulus E'(ε, ω)	Pa•m	$E' = \frac{d\gamma}{\varepsilon}cos\delta$	Report along with the oscillation frequency, strain and interfacial tension [90,97]
Interfacial dilatational loss modulus E"(ε, ω)	Pa•m	$E'' = \frac{d\gamma}{\varepsilon}sin\delta$	Report along with the oscillation frequency, strain and interfacial tension [90,97]
Complex interfacial dilatational modulus E*	N/m	$E^* = E' + iE''$	Report along with the oscillation frequency, strain and interfacial tension [90,97]
Oscillation strain amplitude ε	–	$\varepsilon = \frac{\Delta A}{A_0}$	–
Oscillation frequency ω	rad/s	$\omega = 2\pi f$	f corresponds to the frequency in Hz

2.1.3. Interfacial shear rheology experiments

In interfacial shear rheology, the 2D interfacial layers are subjected to a shear flow field at constant area to determine their resistance to deformation and extract shear viscoelastic properties. The interfacial layers are exposed to sinusoidal shear deformations with a shear strain amplitude γ_s and an oscillation frequency ω to determine the shear storage modulus G_i' and loss modulus G_i":

$$G' = \frac{\sigma_0}{\gamma_s}cos\delta$$

$$G'' = \frac{\sigma_0}{\gamma_s}sin\delta$$

where σ_0 is the shear stress amplitude and $\gamma_s = r\theta_0$, r being the radial distance and θ_0 the maximum deflection angle. A full stress-strain cycle may be depicted in Lissajous plots to understand the behavior of the interfacial layers at critically high strains [93,98]. An important consideration in interfacial shear rheology is that the total shear stress is a combination of interfacial and bulk shear stress as expressed by the dimensionless complex Boussinesq Bo*:

$$Bo^* = \frac{\eta_i^*}{L\eta}$$

where η_i* and η are the complex interfacial viscosity and bulk viscosity, respectively, and L is a characteristic length scale that depends on the used geometry [99–103]. A prerequisite for interfacial shear rheology measurements is that the total shear stress is dominated by interfacial drag rather than by bulk viscosity (Bo* > > 1). A detailed treatment of the importance of Bo*, as well as further operating windows for interfacial shear rheology, is provided by Renggli et al. [104] The obtained total shear stress thus needs to be corrected to obtain the interfacial shear storage G_i' and loss G_i" moduli. Specific approaches for the required corrections have been described for the double wall-ring [105], the bicone geometry [106,107], and magnetic rod rheometers [101,102]. Sánchez-Puga et al. [100,108] provided an open source software package (BiconeDrag, dx.doi.org/10.17632/c245bmgf5n.1) to correct interfacial shear rheology data. For full traceability, we recommend the reporting of dimensions, viscosities, and densities used for the correction, and ideally reporting the uncorrected data (G', G") or total torque and angular displacement to extract G_i' and G_i". An overview of relevant data for interfacial shear rheology measurements and subphase correction is provided in Table 3.

2.1.4. Structural analysis of interfacial layers

Structural analysis on the 2D structure and organization of adsorbed interfacial layers can link observed Π-A isotherms or interfacial rheology to specific interfacial structures. The most suitable technique(s) for structural analyses varies considerably depending on the surface-active species and subphases involved. Adsorbed microparticles may be visualized directly by optical microscopy [109,110], while the structuring and phase transitions of surfactant layers can be visualized by fluorescence or Brewster angle microscopy [111–113]. Other surface-active species, e.g., proteins, nanoparticles, polymers, or polymeric microgels, are often limited to indirect measurements based on dielectric properties (ellipsometry) [114,115] or scattering length density (X-ray or neutron reflectometry) [116–118] that are distinct from either subphase, Langmuir-Schaefer deposition and imaging by atomic force microscopy (AFM) [119], or in situ liquid AFM [120,121]. Commonly extracted data are the surface layer thickness d, surface roughness σ, or surface coverage η. The contact angle θ of adsorbed particles or spreading of microgels can further be obtained from reflectometry [122], gel trapping [123], or freeze-fracture shadow-casting cryo-scanning electron microscopy [124]. In ellipsometry and reflectometry techniques, those quantities are obtained by data fitting, and respective models and fitting parameters have to be meticulously reported. Large

Table 3
Overview of relevant data and metadata for Interfacial shear rheology experiments and subphase correction.

Data	Unit	Equation	Comment
Interfacial shear rheology data			
Interfacial shear storage modulus $G_{is}'(\gamma_0, \omega)$	Pa•m	$G_i' = \frac{\sigma_0}{\gamma_s}cos\delta$	Report along with the oscillation strain and frequency [90,97]
Interfacial shear loss modulus $G_i''(\gamma_0, \omega)$	Pa•m	$G_i'' = \frac{\sigma_0}{\gamma_s}sin\delta$	Report along with the oscillation strain and frequency [90,97]
Complex interfacial shear modulus G_i^*	Pa•m	$G_i^* = G_i' + iG_i''$	Report along with the oscillation strain and frequency [90,97]
Complex interfacial viscosity η_i^*	Pa•s•m	$\eta_i^* = \frac{G_i^*}{i\omega}$	Report along with the oscillation strain and frequency [90,97]
Oscillation strain amplitude γ_s	–	$\gamma_s = r\theta_0$	–
Oscillation frequency ω	rad/s	$\omega = 2\pi f$	–
Data for correction			
Storage modulus G'	Pa	$G' = \frac{\sigma_0}{\gamma_s}cos\delta$	–
Loss modulus G''	Pa	$G'' = \frac{\sigma_0}{\gamma_s}cos\delta$	–
Subphase viscosities η	Pa•s	–	From bulk rheology experiments
Subphase densities ρ	kg/m^3	–	–
Characteristic length scale L	m	–	Depends on used setup/ geometry [99,100,104]
Method metadata			
Method	–	–	Report mode of measurement and instrument details [87,88]
Materials	–	–	Report material and dimensions of used cups and geometries [104]
Surface area A	m^2	–	–
Bulk volume	m^3	–	Particularly relevant if adsorption occurs from a subphase

scale neutron facilities often have established data storage guidelines and transparent data processing workflows in place [125]. Regarding image files, the adequate analysis of images without bias and the open sharing of image files and metadata are a major challenge across research disciplines [126,127]. The unprocessed image files, ideally as OME-TIFF files with rich metadata provided in one file, should be shared alongside all code and processes used for image analysis and data extraction. An overview of relevant data for interfacial structural analyses is provided in Table 4. Due to the diversity of interfacial structural methods, we refer the reader to specialized literature for relevant method metadata.

Table 4
Overview of relevant data for Interfacial structure experiments.

Data	Unit	Equation	Comment
Interfacial structure data			
Structure	–	–	Often qualitative, i.e., order/disorder or detection of impurities in adsorbed surfactant or particle layers. Share respective image files including metadata [126,127]
Layer thickness	m	–	Report used model and fit parameters
Layer roughness	m	–	Report used model and fit parameters
Surface coverage	%	–	Report used model and fit parameters
Contact angle	degree	–	For adsorbed particles

2.2. Metadata – surface-active species

Besides the data related to different interface science experiments, datasets should be complemented with rich metadata to guarantee traceability, reproducibility, and reusability of the data. In interface science experiments, this concerns particularly the detailed description of the surface-active species, the liquid subphases, and experimental conditions used. In the following, we aim to define the metadata to be reported to understand the primary data obtained from interface science experiments.

2.2.1. Surfactants

The term 'surfactant' generally refers to low-molecular weight molecules with a polar headgroup and a hydrophobic tail which renders them surface-active (Fig. 2A). Many surfactants are sold under trademark names (e.g., Tween, Brij) necessitating their unambiguous identification using international chemical identifier (InChI). The self-assembly of surfactants in bulk, and to some degree at liquid interfaces, is correlated to their head and tail geometry, as expressed by the critical packing parameter [128–131]. For surfactant partitioning at fluid interfaces multiple concepts have been proposed over the years, including the spontaneous curvature of adsorbed surfactants [132], phase inversion temperature [133], packing parameter [134], or the Winsor ratio [135], which are unified in the hydrophilic-lipophilic deviation (HLD) from optimum formulation concept which for anionic surfactants reads [136–139]:

$$HLD = f(S) - K(EACN) - f(A) + \sigma_S - a_T(T)$$

where f(S) a function accounting for salinity, K an empirical constant depending on the surfactant headgroup which is a function of the equivalent alkane carbon number (EACN) of the oil, f(A) a term accounting for alcohol type and content, σ_S a surfactant-specific parameter, and a_T the empirical temperature constant. HLD = 0 corresponds to equivalent interactions of surfactants with both subphases and a maximum affinity to partition at the interface, sometimes referred to as 'optimum conditions'. The hydrophilic-lipophilic balance (HLB) of surfactants often is a good predictor for the preferred phase of surfactants [140,141]:

$$HLB = 20 \bullet \frac{M_h}{M}$$

where M_h is the molecular mass of the hydrophilic part of the surfactant and M the total molecular mass. Rather hydrophilic surfactants (HLB ≈ 8-16) tend to form oil-in-water emulsions, while hydrophobic surfactants (HLB ≈ 3-6) tend to stabilize water-in-oil emulsions (Fig. 2B) [142].

The adsorption of surfactants at fluid interfaces is generally fast, reversible, and not associated with changes in molecular structure (although complex supramolecular structures are possible under confinement [146,147]). A lot of relevant information on surfactant adsorption can thus be obtained from adsorption isotherms. The surfactant concentration at which no more changes in γ are measured corresponds to the critical micelle concentration (CMC) of a surfactant under the given measuring conditions (or critical aggregation concentration (CAC) for phospholipids). Commercial surfactants are often not pure and may be mixtures, which results in inconsistent behavior or a minimum in adsorption isotherms close to the CMC [148]. The corresponding minimum surface tension, γ_{CMC}, is limited by the surfactant structure and its maximum surface excess Γ_{max} [149–153]. In practice, there often remains an ambiguity about how to quantify the surface activity of surfactants, i.e., by the minimum concentration that leads to a measurable reduction in γ, the CMC, or γ_{CMC} [142]. Hence, ideally both CMC and γ_{CMC} should be reported to facilitate the comparison of surfactant adsorption. Hödl et al. [49] demonstrated that a graph neural network trained with several hundred partially incomplete datasets can

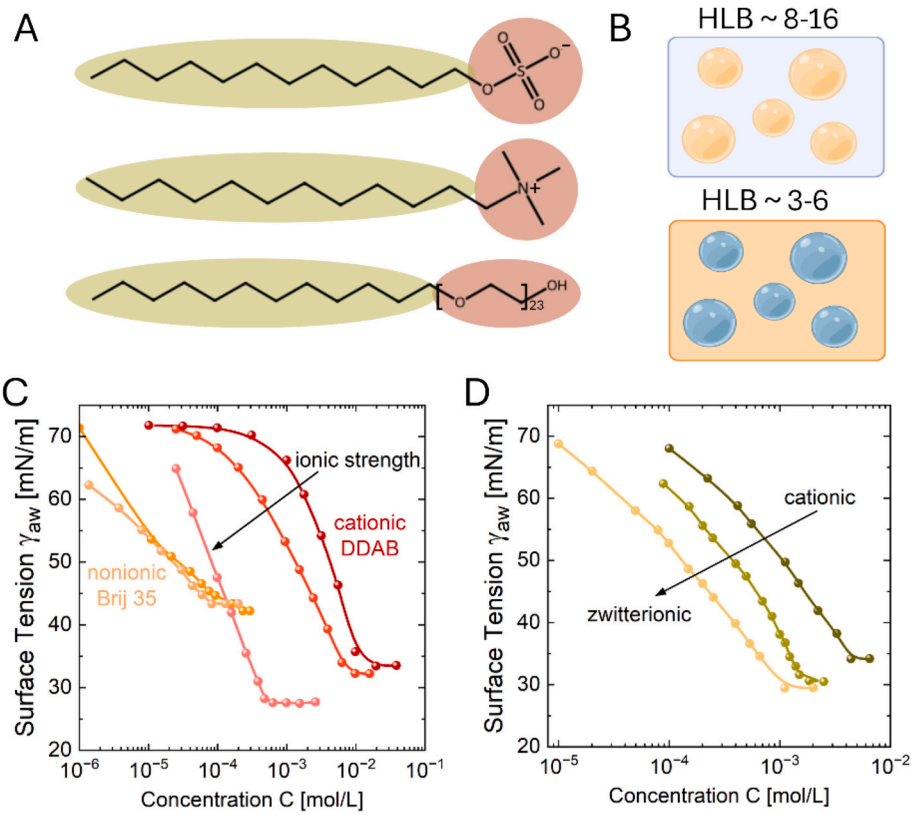


Fig. 2. A) Line notation (SMILES) of anionic sodium dodecyl sulfate (SDS), cationic dodecyltrimethylammonium bromide (DTAB), and polyoxyethylene-(23)-monododecyl ether (Brij 35) visualizing polar headgroups (red) and hydrophobic tail (green). B) Effect of hydrophilic-lipophilic balance (HLB) on emulsification. C) Adsorption isotherms of nonionic (Brij 35) and cationic dodecyldimethylammonium bromide (DDAB) at 0, 0.1, and 1 M NaBr at the a/w surface. Two datasets, from Bergfreund et al. (Ref. 41 and Pisaev et al. (Ref. 143 were replotted for Brij 35 and from Okuda et al. (Ref. 144 for DDAB as a function of ionic strength. D) Adsorption isotherms of ampholytic N-Dodecyl-β-alanine at varying pH in its cationic state (pH 1.5), close to its pK_a (pH 3) and in zwitterionic state (pH 6). Replotted from Nakamura et al. (Ref. 145. (For interpretation of the references to colour in this figure legend, the reader is referred to the web version of this article.)

predict missing information (e.g, CMC, γ_{CMC}, Γ_{max}) based on surfactant structure. This underlines the possibilities of FAIR sharing and reuse of interface science data in combination with machine learning, particularly for surfactants who have a clear correlation of their structure and interfacial assembly. There even is a first example of fully autonomous acquisition and machine learning driven analysis of surfactant adsorption isotherms [154].

For ideal solution behavior, changes in γ can be related to the surfactant surface excess Γ (mol/m^2) by the Gibbs adsorption isotherm [155,156]:

$$\Gamma = -\frac{1}{RTm}\frac{d\gamma}{dlnC}$$

where R is the ideal gas constant, T the temperature and m a parameter taking the charge of the adsorbed surfactant into account. For ideal monolayers of non-interacting surfactants, the affinity of surfactants to partition at the interface in the form of the empirical adsorption equilibrium constant K can be extracted from the Langmuir model [38,157]:

$$\theta = \frac{KC}{1+KC}$$

Here, θ is the fractional surface coverage ($0 \leq \theta \leq 1$). Besides nonionic surfactants, there are anionic, cationic, zwitterionic or mixed 'catanionic' surfactants, whose ionic interactions affect their interfacial packing and CMC. The prefactor m in the Gibbs adsorption isotherm can account for nonionic (m = 1) and ionic (m = 2) surfactants [155,156]. Note that the charge of surfactants depends on their pK_a and respective solution pH. For high ionic strength in the aqueous phase, charged surfactants approximate the behavior of nonionic surfactants (m = 1). In case of considerable electrostatic or steric surfactant interactions, more complex models that account for non-ideality should be considered, as elaborated in detail elsewhere [34,158].

Experimentally, it is observed that nonionic surfactants, e.g. Brij 35, reduce γ at lower concentrations, frequently making it difficult to measure a plateau region without changes in γ (Fig. 2C) [41,143]. Ionic surfactants such as cationic dodecyldimethylammonium bromide (DDAB) generally require higher concentrations to reduce γ and have a higher CMC. However, their adsorption isotherm and CMC are shifted to lower concentrations at increasing ionic strength and approximate the behavior of nonionic surfactants (Fig. 2C) [144,159]. Similarly, the adsorption isotherm of surfactants with pH-dependent ionization can shift depending on pH (Fig. 2D) [145,160]. The adsorption of ionic surfactants thus depends on the aqueous subphase pH and ionic strength, as discussed further below. Surfactant adsorption kinetics are less frequently investigated compared to their isotherms, although they can be useful to extract information on such adsorption barriers of charged surfactants [37,38,161,162]. Viscoelastic properties of interfacial surfactant layers are often negligible and below the threshold of most shear rheometers in the nPa/m range [103]. An overview of relevant data and metadata for surfactants in interface science experiments is provided in Table 5.

2.2.2. *Proteins*

The adsorption behavior of proteins is more complex compared to most other surface-active species, as their adsorption can be associated with long-time intra- and intermolecular structural rearrangements. Adsorbed proteins interact with each other and with proteins in the bulk and may form solid-like layers (arrested states such as two-dimensional

Table 5
Overview of relevant metadata for surfactants in interface science experiments.

Data	Unit	Equation	Comment
Surfactant data & metadata			
Name & molecular structure	–	–	Line notation (SMILES) and InChI. Report potential ionic nature of surfactants. Report purity and composition for commercial surfactants that are mixtures
Concentration C	mol/L	–	–
Critical micelle concentration CMC	mol/L	–	From adsorption isotherm. Alternatively, CAC for phospholipids [142]
Interfacial tension at the CMC γ_{CMC}	N/m	–	From adsorption isotherm [142]
Surface excess Γ	mol/m^2	$\Gamma = -\frac{1}{RTm}\frac{d\gamma}{dlnC}$	From adsorption isotherm [155,156,159,163]
Adsorption equilibrium constant K	L/mol	$\theta = \frac{KC}{1+KC}$	Use alternative model in case of considerable surfactant interactions [34,158]

jammed or gelled states) or aggregated multilayers, often making their adsorption quasi-irreversible [164–170]. Due to this complexity of protein adsorption, including long-timescale structural changes and formation of solid-like layers, transient changes of protein interfacial layers in terms of adsorption kinetics γ(t) or interfacial rheology (E', E"; G_i', G_i") as a function of time, frequency, or deformation amplitude are more frequently investigated. Furthermore, the adsorption of proteins is affected considerably by their extraction procedure. Meticulous sharing of extraction and experimental conditions is thus particularly important for interfacial experiments with proteins to guarantee comparability and reproducibility of results.

2.2.2.1. In-house protein extraction and characterization. While proteins from whey, egg white, or soy have been well studied and characterized for decades and are commercially available as purified isolates from chemical suppliers, proteins from less common sources are often extracted using laboratory-specific extraction protocols and purification procedures. This is a particular challenge regarding the current trend of investigating novel plant or unicellular protein extracts, as it results in variations in the extracted protein content, fractions, and aggregation state from the same raw material (Fig. 3A) [171–175]. For in-house protein extraction, it is thus highly relevant to report the detailed extraction protocol and adequately characterize the obtained protein concentrate in terms of protein content (i.e., nitrogen measurement and reporting of used nitrogen conversion factors), compositional analysis, and confirmation of specific protein fractions using SDS-PAGE, size exclusion chromatography, or high-performance liquid chromatography [176].

2.2.2.2. Protein adsorption: several subprocesses limited by protein structure and mobility. The adsorption of proteins at fluid interfaces often leads to the formation of solid-like films that evolve over time due to in-plane rearrangements (aging), potentially associated with changes in protein secondary or tertiary structure. These processes result in measurable changes in γ or interfacial viscoelasticity over several hours to days, making adsorption experiments as a function of time more relevant for proteins. Benjamins et al. [170] and later Graham and Phillips [182–184] introduced the concept that protein adsorption can be described as a series of subprocesses, including I) diffusion-limited migration to the interface, II) penetration, III) interfacial rearrangement, and potentially IV) multilayer formation. Steps II-IV are limited by the proteins' mobility and protein intermolecular interactions in the interfacial plane. The latter is limited by the proteins' structural stability and leads to pronounced differences in adsorption kinetics for unstructured ('random coil') compared to structured ('globular') proteins [26,165,185–189], as visualized for random coil β-casein and highly stable globular lysozyme in Fig. 3B. This structural limitation of globular protein adsorption is reduced in case of partial denaturation or hydrolysis of proteins, and it is thus crucial to report processing steps like heating or acid/base treatments that can potentially induce protein denaturation or hydrolysis [165,190–194].

2.2.2.3. Protein amphoterism makes their adsorption pH and ionic strength dependent. Proteins are ampholytic and their behavior in bulk and at the interface varies considerably based on the aqueous subphase pH and ionic strength. Most proteins contain both potentially cationic and anionic amino acids, making their net charge and effective ζ-potential a function of pH with a characteristic isoelectric point pI with zero net charge (Fig. 3C). Many established animal-based proteins from milk as well as proteins from legumes have a pI in the range of ≈ 4-5 [177,178]. However, notable exceptions exist such as lysozyme (pI ≈ 10-11) [179] or proteins from certain microalgae strains which have an exceptionally low pI ≈ 2-3 [180]. Protein adsorption is favored and primarily diffusion-limited at low net charge, i.e., close to their isoelectric point or increased ionic strength, due to less electrostatic repulsion between and within proteins. However, proteins may lose their surface-activity if their ζ-potential is too low due to bulk aggregation and precipitation [181,195–198]. This behavior is exemplified in Fig. 3D for β-lactoglobulin [181]. At low concentrations (5×10^{-6} mM), adsorption is impaired at the pI compared to pH 7 due to reduced protein solubility. However, at high protein concentration (10^{-2} mM) adsorption is faster at the pI due to the excess protein. Similarly, β-lactoglobulin adsorption is enhanced at increased ionic strength (Fig. 3E).

In summary, for experiments involving proteins, it is pivotal to report a rich set of metadata including their composition and purity, (multimeric) structure and stability, potential pretreatments, and their ζ-potential or net charge and resulting solubility S under the aqueous subphase conditions. For protein mixtures, it is important to report the composition and properties of individual protein fractions. An overview of relevant metadata for proteins in interface science experiments is provided in Table 6.

2.2.3. Polymers

There are several synthetic polymers that exhibit surface-activity such as polyethylene oxide (PEO), partially hydrolyzed polyvinyl alcohol, partially ionized acrylic acid, or hydrophobically modified polyacrylamide [200–203]. Polymer adsorption is primarily affected by their molecular weight M_w and degree of polymerization DP, which corresponds to M_w/M_u where M_u is the molecular weight of the monomer. Generally smaller polymers adsorb faster due to a higher diffusion coefficient and fewer conformational rearrangements, however, larger polymers adsorb more strongly due to increased contact points and lower entropy loss per segment on adsorption [204–207]. The focus of experimental interface science has been on complex amphiphilic polymers in the past decades, specifically block copolymers and, more recently, bottlebrush copolymers.

2.2.3.1. Block copolymers. Block copolymers consist of blocks of different synthetic polymers, typically a more hydrophilic (A) and a more hydrophobic (B) one. They adsorb at fluid interfaces due to the different solvent selectivity of each block, which together with interblock segregation makes the interface the thermodynamically favorable location following Flory-Huggins' solution theory [208,209]. Block copolymers commonly investigated for interfacial partitioning are diblock copolymers (A-B) or triblock copolymers (A-B-A, B-A-B). A particularly widely investigated family of copolymers are poloxamers (Pluronics) consisting of a hydrophobic chain of polyoxypropylene (poly (propylene oxide)) (PPO) flanked by two hydrophilic chains of PEO. The surface pressure of copolymers follows a scaling law [210–212]:

$$\Pi \cong k_B T \Gamma^{y}$$

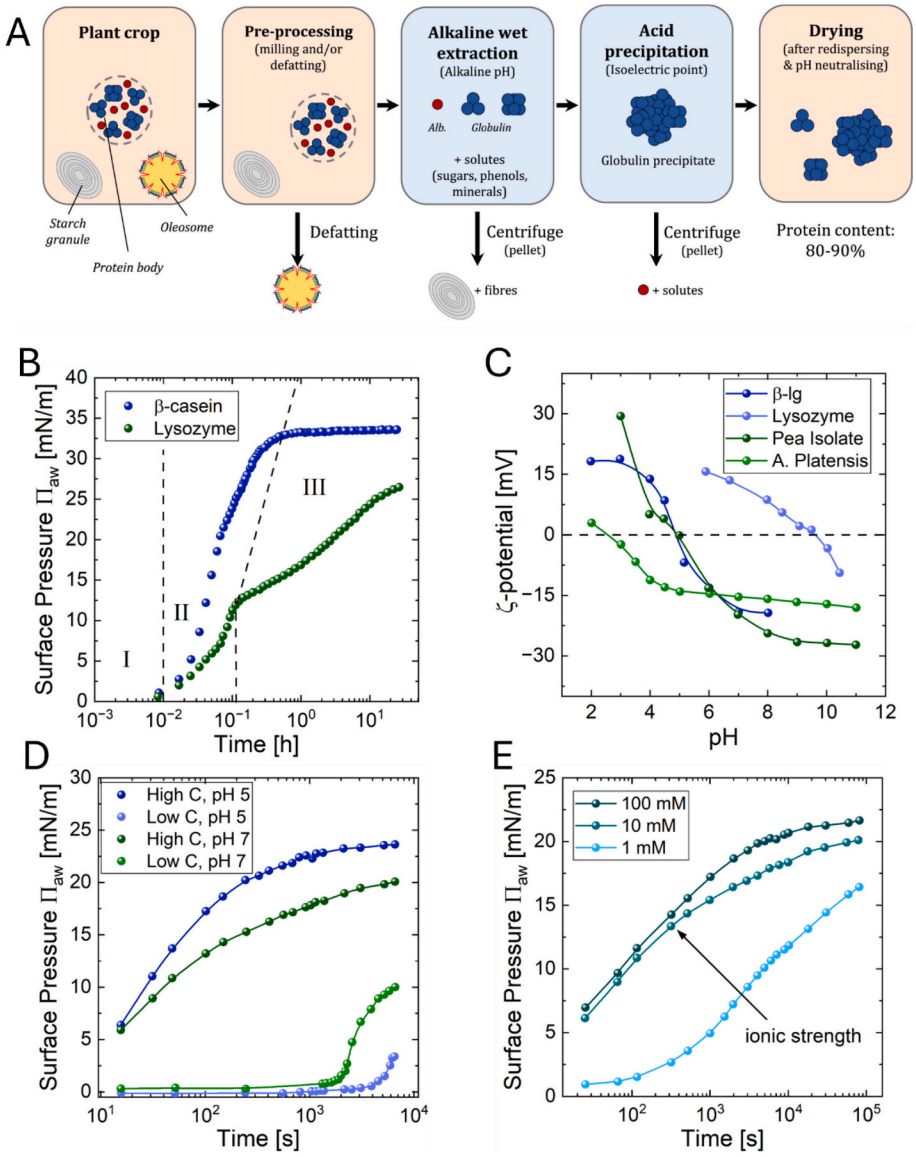


Fig. 3. A) Example for step-by-step purification from biomass to protein powder by wet fractionation. Reprinted with permission from Yang et al. (Ref. 175. B) Adsorption kinetics of random-coil β-casein and globular lysozyme at the a/w interface. Replotted from Freer et al. (Ref. 26. C) ζ-potential as a function of pH for β-lactoglobulin (Bertsch et al., Ref. 177, pea protein isolate (Tang et al., Ref. 178, lysozyme (Kubiak-Ossowska et al., Ref. 179, and *A. platensis* isolate (Böcker et al., Ref. 180. D) Adsorption kinetics of β-lactoglobulin at the a/w interface at varying concentration at pH 7 and close to its isoelectric point (≈ 5) and E) at increasing ionic strength. Replotted from Ulaganathan et al. (Ref. 181.

where k_B is the Boltzmann constant and y is a scaling parameter describing the solvent quality of the interface for the copolymer. At increasing Γ block copolymers experience several structural transitions as evidenced by ellipsometry and manifested by distinct regimes in elasticity versus.

Π plots (Fig. 4A). In the dilute regime (I), copolymers adsorb in a two-dimensional stretched chain conformation in the interfacial plane with a linear increase of the limiting elasticity E_0 with y = 2 (stretched chains) [213,214]:

$$E_0 = y\Pi$$

Copolymers may form self-assembled disk or worm-like structures in this dilute regime, depending on block structure [216]. At the critical overlap surface concentration (II), some of the hydrophilic blocks are forced to extend into the aqueous subphase, leading to a drop in E* due to inhomogeneous polymer conformations. At further increasing surface load (III) E* increases again due to the formation of compact and homogeneous 3D structures, where the hydrophobic block acts as an anchoring point at the interface, and the hydrophilic block(s) extend into the aqueous subphase. The hydrophilic blocks may loosely extend into the aqueous phase as coils with some overlap ('mushroom') or stretch out if overlap is energetically costly, i.e., in a good solvent ('brush') [115,217–219]. Hydrophobic block copolymers may experience a further decrease in E_0 (IV), which may be attributable to the expulsion of the hydrophobic block into the aqueous phase or the coexistence of mushroom and brush structures [213,214]. In a similar fashion, these structural transitions can also be observed in the corresponding Π-A isotherms [219–221].

Regarding adsorption kinetics, block copolymer adsorption is limited by diffusion and an adsorption barrier due to chain reorientation at low Γ [215,217]. At the onset concentration of brush formation c_1 adsorption is further limited by reorganization into brush structures, and adsorption kinetics are best described by a combined diffusion plus reorientation model. Beyond c_1 diffusion is no longer limiting; the surface is rapidly saturated and further adsorption is limited by the

Table 6
Overview of relevant metadata for proteins in interface science experiments.

Data	Unit	Equation	Comment
Proteins metadata			
Name	–	–	For in-house extraction, report isolation protocol and expected fractions supported by SDS-PAGE [175]
Concentration C	kg/L	–	Report protein content for extracts and individual concentrations in protein mixtures [175]
Purity (protein content)	–	–	For in-house extraction, report protein content, composition, and determination method, e.g., Dumas or Kjeldahl method, and used nitrogen conversion factor [175]
Molecular weight M_w	g/mol (Da)	–	Obtained from SDS-PAGE or SEC [176]
Size in solution	m		Radius of gyration or hydrodynamic radius from scattering experiments
Structure	–	–	Globular or random coil structure, if known multimeric structure or aggregation state [26]
Thermodynamic stability ΔG_u (Folded ⇆ Unfolded)	J/mol	–	Relevant for globular protein adsorption [30,199]
Denaturation/Hydrolysis	–	–	Report pretreatments (heat, pressure, acid/base) that may affect protein structure and ideally quantify, e.g., by DSC, CD, FTIR, or SDS-PAGE [165,190–194]
Isoelectric point pI	–	–	In protein mixtures, experimental determination (ζ-potential) typically provides pI of major fractions
ζ-potential (pH, I)	V	–	Report for relevant buffer pH and ionic strength
Net charge (pH)	–	–	–
Solubility S (pH, I)	kg/L	–	Determined by colorimetric assay of supernatant or nitrogen solubility [180]

reorganization of adsorbed copolymers which can lead to a temporary stagnation of γ(t) (**Fig. 4 4B**) [215].

The benefit of synthetic block copolymers in terms of metadata reporting is that their monomer number and block sequence (e.g., PEO_x-PPO_y-PEO_x), which mostly determine their interfacial behavior, are generally known. The ratio of hydrophilic and hydrophobic monomers N_B/N_A can provide a rough approximation of the hydrophilic-hydrophobic balance of block copolymers, but a better estimate is provided by the ratio of the Flory radii R_F of hydrophilic and hydrophobic blocks [115]:

$$\beta = \frac{R_F^{(B)}}{R_F^{(A)}} = \frac{l_B}{l_A}\left(\frac{N_B}{N_A}\right)^{3/5}$$

where l_i is the length and N_i the number of monomers of hydrophilic blocks A and hydrophobic blocks B.

2.2.3.2. Bottlebrush copolymers. Bottlebrush copolymers, linear polymers grafted with polymeric sidechains of altering hydrophobicity, have recently been increasingly investigated for their interfacial assembly. For bottlebrush copolymers, reporting of the backbone degree of polymerization N_{BB}, degree of sidechain polymerization N_{SC}, grafting density (sidechain repeat units/backbone repeat units), as well as dispersity and compositional heterogeneity are relevant to their interfacial assembly, structure, and rheology [222–226]. Bottlebrush copolymers form denser interfacial layers with lower γ_{eq} for shorter backbones and a higher degree of hydrophobic side chains [224–227]. Higher packing and lower γ_{eq} is further favored by a blockwise distribution of hydrophilic and hydrophobic sidechains compared to random distributions [226]. An overview of relevant metadata for copolymers in interface science experiments is provided in Table 7.

2.2.4. Surface-active polysaccharides

Most polysaccharides are not inherently surface-active, however, there are a few examples of naturally occurring polysaccharides which are surface-active due to peptide side-chains, such as gum Arabic or sugar beet pectin [228–232]. Furthermore, some polysaccharides are frequently modified to be surface-active, such as hydrophobically modified starch [228,233] or dextran [234], methylcellulose [235], and hydroxypropyl methylcellulose [231,236]. Due to natural variations and different modification protocols, it is critical to report the structure and characteristics of the used polysaccharides, such as their average M_w and dispersity, e.g., by high-performance size-exclusion chromatography [237,238], as well as the monosaccharide composition and the density and distribution of hydrophobic groups. A practical guide for polysaccharide hydrolysis and monosaccharide determination was provided by Liu et al. [239] Furthermore, the charge density obtained from conductometric titration [240] and ζ-potential as a function of pH and ionic strength in solution are important parameters for charged polysaccharides. An overview of relevant metadata for polymers in interface science experiments is provided in Table 8. A recent trend is the formation of microgel particles from surface-active polysaccharides, which

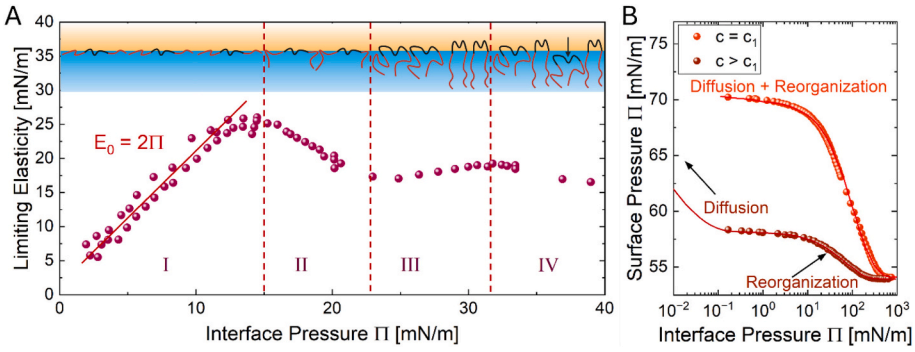


Fig. 4. Limiting elasticity E_0 as a function of o/w interfacial pressure of triblock copolymers showing different characteristic regimes due to interfacial transitions from I) 2D stretched chains (y = 2), II) overlap and extension into aqueous phase, III) formation of ordered 3D mushroom or brush structures, and potentially IV) expulsion of copolymers into the aqueous phase or coexistence of mushroom and brush structures. Replotted from Ramírez et al. (Ref. 214. B) Adsorption kinetics of triblock copolymers at the a/w surface at the onset concentration of brush formation c_1 and at $c > c_1$ showing the transition from diffusion- to reorganization-limited adsorption. Replotted from Muñoz et al. (Ref. 215. Created in BioRender. Bertsch, P. (2026) https://BioRender.com/x988b5f.

Table 7
Overview of relevant metadata for polymers in interface science experiments.

Data	Unit	Equation	Comment
Polymer metadata			
Monomer name(s)	–	–	–
Concentration C	mol/L	–	–
Molecular weight M_w	g/mol (Da)	–	Include information on dispersity [204]
Degree of polymerization	–	$DP = \frac{M_w}{M_u}$	–
Block copolymers (additional considerations)			
Block structure	–	–	Report number of monomers and block sequence, e.g., PEO_x-PPO_y-PEO_x [115]
Hydrophobicity (Flory radii ratio β)	–	$\beta = \frac{R_F^{(B)}}{R_F^{(A)}} = \frac{l_B}{l_A}\left(\frac{N_B}{N_A}\right)^{3/5}$	Hydrophilic/hydrophobic monomer ratio N_B/N_A can provide rough estimate [115]
Bottlebrush copolymers (additional considerations)			
Degree of polymerization	–	–	Report for backbone (N_{BB}) and sidechains (N_{SC}) [226]
Grafting density	–	–	Sidechain/backbone repeat units [226]

are themselves surface-active and behave as soft particles at fluid interfaces [241], and are discussed further below.

2.2.5. Solid (nano)particles

2.2.5.1. Micron-sized particles. Solid particles, despite not being amphiphilic, can still accumulate at fluid-fluid interfaces if the contact between the particle and the subphases is energetically more favorable compared to the direct contact of the subphases [242–244]. The interfacial adsorption energy E_{ad} of solid particles is given by:

$$E_{ad} = -A\gamma_{ow}(1 + cos\theta_{ow})^2$$

where A is the o/w interfacial area eliminated by the particle, and θ_{ow} is the contact angle of the particle with the o/w interface, which results from the wettability of the solid particle by the water and oil subphase according to Young's equation (Fig. 5A):

$$cos\theta_{ow} = \frac{\gamma_{so} - \gamma_{sw}}{\gamma_{ow}}$$

Hence, the adsorption energy and positioning of solid spherical particles at fluid interfaces can be fully described by reporting particle dimensions, solid-fluid contact angles, and γ_{ow} [249–254]. The adsorption energy of spherical particles is a function of θ and their size ($A = \pi r^2$ at $\theta = 90°$) and is usually irreversible with high adsorption energies ($E_{ad} >> 10^3$ k_BT) for micron-sized particles (Fig. 5B). For charged particles, subphase conditions beyond wetting can be relevant for adsorption, such as the pH and ionic strength of the aqueous phase that determine the magnitude of electrostatic interactions [255], or the relative permittivity ε_r of the oil which determines long-range Coulombic repulsion through the oil phase [256,257]. A high particle surface charge can prevent adsorption due to electrostatic repulsion between particles, adsorbed ions, and image charge effects at the interface [243,257–260]. Besides the surface chemistry and size, the surface morphology can also play an important role and should be reported accordingly. To a certain extent, an increase in surface roughness or chemical patchiness can enhance the wettability of particles by both the hydrophilic and hydrophobic subphase, allowing for higher adsorption energies, and particles that can stabilize both o/w and w/o emulsions [261–264]. Although θ can be estimated by Young's equation, experimental determinations remain important due to particle size dispersity, surface heterogeneities, contact angle hysteresis and kinetic effects [123,124].

The matter is more complicated for non-spherical particles, such as ellipsoids, oblates, or cylinders that orient in the interface plane and induce anisotropic interface deformations, i.e., variations of θ_{ow} along the contact line of the particles [265]. Depending on geometry (ellipsoid vs. cylinder) and surface chemistry, this results in a depression of the interface contact line along the sides of particles and a rise at the tips, or vice versa (Fig. 5C) [266–268]. These anisotropic interface deformations induce lateral capillary forces between particles that favor a side-by-side or tip-to-tip orientation (**Fig. 5D** and **E**) [109,110,246,247,269–274]. Adsorbed anisotropic particles are further destabilized by line tension along their long axis, which results in a lower θ than predicted by Young's equation which demands a correction term (Fig. 5F) [245,275,276].

2.2.5.2. Considerations for nanoparticles. Some considerations for solid particle adsorption need to be revisited for nanoparticles. Due to their smaller size, nanoparticles and their adsorption are subjected to diffusion as described by a modified Ward-Tordai model [277]. They need to overcome a considerable energy barrier for adsorption particularly in case of hydrophilic or charged nanoparticles [278,279]. The adsorption energy of nanosized particles is much lower in the range of ~ k_BT depending on size, adsorption angle, and γ_{ow} (Fig. 5G), allowing for nanoparticle desorption [79,280]. Determination of adsorption energies using the standard capillary approach can fail for nanoparticles due to the finite thickness and adsorption-induced curvature of the interface that can be at relevant length scales for nanoparticles. The E_{ad} of nanoparticles is better approximated by an interfacial displacement approach [79,281]:

$$E_{ad} = -\frac{A}{\gamma_{ow}}(\gamma_{ow}(\gamma_{sw} - \gamma_{so}))^2 = -\frac{\Pi A}{\eta_s}$$

The second term exploits the fact that nanoparticles, unlike most micrometer sized particles, induce considerable changes in interfacial tension and their adsorption energy can thus be approximated experimentally from changes in γ and determination of their surface coverage η_s. Due to the increasing adsorption energy as a function of size, the adsorption kinetics and γ_{ow} reduction are enhanced for larger nanoparticles (Fig. 5H) [248]. The lower adsorption energy makes nanoparticle adsorption susceptible to effects that counteract adsorption like electrostatic repulsion, low γ_{ow}, already adsorbed particles, or line tension in case of anisotropic nanoparticles [276,282–287]. As a result, the adsorption of charged nanoparticles can be slow, particularly at polar oils with low γ_{ow}, but may be enhanced by an increase in ionic strength that reduces electrostatic repulsion (Fig. 5I) [76]. An overview of relevant metadata for particles in interface science experiments is provided

Table 8
Overview of relevant metadata for surface-active polysaccharides in interface science experiments.

Data	Unit	Equation	Comment
Surface-active polysaccharides metadata			
Concentration C	mol/L	–	–
Source and extraction/modification procedure	–	–	For in-house extraction, report isolation protocol and composition (purity)
Structure	–	–	Report backbone and side chain monosaccharides, density and distribution of sidechains [239]
Molecular weight M_w	g/mol (Da)	–	Include information on dispersity [237,238],
Charge density	mol/g	–	From conductometric titration [240]
ζ-potential (pH, I)	V	–	For charged polysaccharides

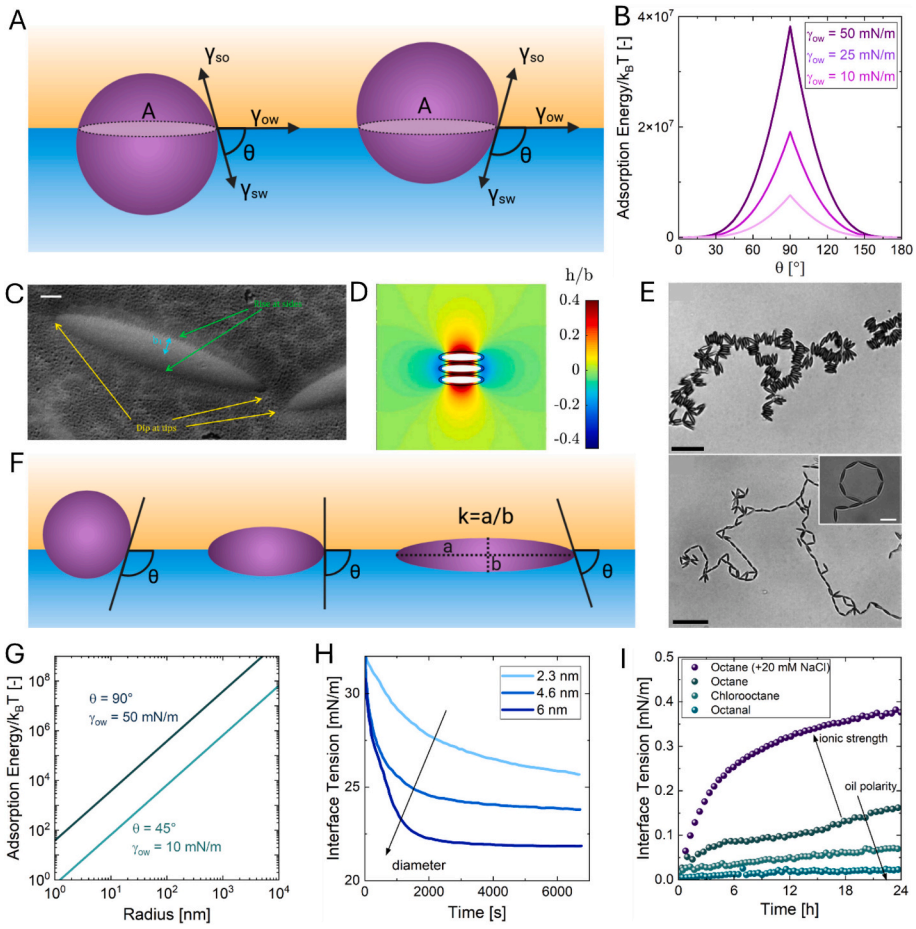


Fig. 5. *A) Schematic of solid particle adsorption at a fluid-fluid interface at contact angle* θ *given by particle wetting by both subphases and interfacial tension* γ_{ow}. *B) Adsorption energy for a r = 1* μm *spherical particle as a function of* θ *at oils with altering* γ_{ow}. *C) Freeze-fracture shadow-casting cryo-SEM image visualizing the interface rise along the side and dip at the tips of an ellipsoid adsorbed at the decane/water interface. The scale bare corresponds to 200 nm. Reprinted with permission from Coertjens* et al. *(Ref. 245 D) Simulation of meniscus deformation relative to particle width h/b of adsorbed ellipsoids (k = 4,* θ *= 40°) favoring lateral alignment. Reprinted with permission from Luo* et al. *(Ref. 246. Optical microscopy images of ellipsoidal particles (k = 4.2) at the o/w interface favoring side-to-side (silica) or tip-to-tip (polystyrene) orientation depending on surface chemistry (scale bar = 50* μm*). Reprinted with permission from Loudet* et al. *(Ref. 247 F) Schematic effect of particle aspect ratio k on* θ. *G) Adsorption energy of spherical particle as a function of radius for two different scenarios of* θ *and* γ_{ow}. *H) Adsorption kinetics of spherical cadmium selenide nanoparticles of different size. Replotted from Kutuzov* et al. *(Ref. 248. I) Adsorption kinetics of negatively charged nanoparticles at oils with increasing polarity,* i.e., *decreasing* γ_{ow}, *and upon increasing ionic strength. Replotted from Bergfreund* et al. *(Ref. 76. Created in BioRender. Bertsch, P. (2026) https://BioRender.com/4qbxijf.*

in Table 9.

2.2.6. Soft particles

Soft particles, i.e., synthetic and biopolymeric microgels, have attracted interest in interface science due to their particular interfacial behavior. The major differences compared to solid particles discussed above are i) that they swell in either bulk phase and can adopt an asymmetric shape at fluid interfaces and ii) their soft-solid nature allows a certain spreading of the particles at the interface based on a competition of interfacial stresses and particle elasticity [288,289]. It is important to note that the term 'microgel' is used for two classes of sub-millimeter (frequently even sub-micrometer), soft-solid polymer aggregates which differ significantly in their preparation and properties. On the one hand, polymeric microgels can be produced by cross-linking of synthetic monomers. On the other hand, soft particles based on biopolymers are produced by bottom-up (aggregation, precipitation) or top-down (breaking of macroscopic cross-linked hydrogels) preparation. Polymeric microgels with their characteristic core-shell structure adopt a 'fried- egg' shape at fluid interfaces. The heat or pH-induced aggregation of biopolymers, or particularly the top-down breaking of macroscopic hydrogels often results in less uniform micron-sized gel particles that can deform and adopt a lenticular shape at fluid interfaces based on particle wetting, interfacial stresses, and particle elasticity E (Fig. 6A-E). Their positioning and spreading at a fluid interface (assuming perfectly soft particles with negligible elasticity) is given by the wetting of the particle by each subphase and the interfacial tension following Neuman's triangle construction (Fig. 6F) [254]. The major discrepancies between 'synthetic' and 'biopolymeric' microgels in bulk and at interfaces were recently reviewed by Akgonullu et al. [241]

2.2.6.1. Synthetic microgels. Cross-linking of synthetic monomers, such as commonly investigated poly(N-isopropylacrylamide) (pNIPAM) [293], leads to microgels with a dense core of highly cross-linked polymer and a looser polymer corona. At fluid interfaces, such microgels adapt an asymmetric 'fried-egg' shape characterized by the dense core, a loosely extended polymer corona in the aqueous bulk phase and interfacial plane, and collapsed polymer chains in the bulk oil or gas phase [121,294–296]. Tuning the polymerization protocol allows the modulation of microgel size and stiffness [290,297,298], whilst the polymerization around a solid inorganic core can be employed to obtain core-shell particles [299,300], anisotropic [300] or hollow microgels [300–302]. As the polymers are temperature sensitive, the respective microgels exhibit a volume phase transition temperature (VPTT), e.g., ≈ 32 °C for pNIPAM. Microgels are thus swelling, soft, and compressible

Table 9
Overview of relevant metadata for particles in interface science experiments.

Data	Unit	Equation	Comment
Solid particles metadata			
Concentration C	kg/L	–	–
Particle dimensions and shape	m	–	Report relevant particle shape to determine interfacial area A and aspect ratio k for anisotropic particles [245,268]. Include information on dispersity
Surface chemistry, subphase contact angle	rad	$cos\theta_{ow} = \frac{\gamma_{so} - \gamma_{sw}}{\gamma_{ow}}$	Report contact angle Report particle contact angle and details on measuring technique used [123,124] Report chemical patchiness [264] Consider correction term for anisotropic particles accounting for line tension [245]
Adsorption energy E_{ad}	J	$E_{ad} = -A\gamma_{ow}(1 + cos\theta_{ow})^2$ $E_{ad} = -\frac{A}{\gamma_{ow}}(\gamma_{ow}(\gamma_{sw} - \gamma_{so}))^2$	Use second term if contact angle approach fails, e.g., for nanoparticles [79]
Surface roughness	μm	–	Report in μm if possible or otherwise qualitatively, e.g., by imaging [262]
ζ-potential (pH, I)	V	–	Report for relevant buffer pH and ionic strength

above, and rigid below their VPTT [296,303]. The use of charged microgels affects their adsorption and lattice structure at high surface coverage or under compression [304,305]. Synthetic microgels are usually synthesized in-house, requiring detailed reporting of the polymerization procedure and the characteristics of the particles obtained in terms of their size and crosslinker content. The internal polymer density profile, which affects conformations after adsorption, can be obtained by small-angle X-rays or neutron scattering or static light scattering depending on particle size [121,302]. Purification after synthesis through dialysis and/or supernatant exchange is required for the removal of surface-active impurities that influence the adsorption kinetics and interfacial reorganization [306].

The aqueous subphase affects the microgel interfacial behavior in terms of polymer extension into the water phase and compressibility of microgel layers [296]. Regarding the hydrophobic subphase, more hydrophobic oils with a high γ_{ow} promote a wider spreading of the microgels in the interfacial plane and less extension into the oil phase [297,307]. Oils with low γ_{ow} decrease the microgel stretching on the interface plane, while the use of organic phases in which the polymer solubility is significantly enhanced (e.g., fatty alcohols) facilitates the swelling into the organic phase (Fig. 6B) [121,308].

2.2.6.2. Biopolymeric hydrogels. Microgels can be obtained from proteins or polysaccharides by bottom-up assembly or top-down breaking of macroscopic hydrogels. Particularly the latter leads to microgel particles that are non-uniform in size, shape and stiffness [291,309–312]. A precise numerical treatment of biopolymeric microparticles is usually not possible due to their heterogeneous size, shape and stiffness. However, uniform microgels in smaller quantities can be obtained by microfluidics (Fig. 6E) [292]. Biopolymeric microgels are often fabricated from surface-active biopolymers like proteins or sugar-beet pectin, and it is assumed that their amphiphilic nature contributes to the adsorption of resulting microgels [313]. However, microgels obtained from non-surface-active polysaccharides still accumulate at interfaces as soft particles [312]. It is thus important to report the biopolymer source and microgel formation procedure and, best as possible, their size, shape, and stiffness distribution. An overview of relevant metadata for microgels in interface science experiments is provided in Table 10.

2.3. Metadata – surface-active species

2.3.1. Aqueous phase

Many surface-active species are dispersed or dissolved in the aqueous phase and adsorb from there at the fluid a/w or o/w interface. Hence, it is pivotal to meticulously report the aqueous phase conditions in terms of the used temperature, pH, ionic strength, and employed buffer salts. The CMC of ionic surfactants decreases as a function of ionic strength (**Fig. 2C** and **D**) [142,314–316]. The surface-activity of proteins generally increases near their pI or at increased ionic strength due to decreased interfacial electrostatic repulsion and aqueous solubility, but is impaired upon precipitation at their pI (**Fig. 3F** and **G**) [181,195–197]. The effect of buffer ion on the adsorption of proteins [317,318] and surfactants [319,320] can follow a Hofmeister series or a reversed Hofmeister series depending on protein charge. For microparticles with charged surface groups, adsorption also depends on the aqueous phase pH and ionic strength [255]. Particularly the adsorption of nanoparticles with lower E_{ad} can be sensitive to electrostatic repulsion at the interface, and adsorb more readily at increased ionic strength (Fig. 5I) [76,285,286]. For all interfacial measurements, even small amounts of surface-active contaminants present in the aqueous phase, e.g., introduced via insufficiently purified materials or contaminated labware, can considerably affect interfacial experiments. A measurement of the clean air-water surface tension γ_{aw} ($\approx$ 72.4 mN/m at 20 °C) that remains constant for several minutes is good practice prior to each experiment to confirm the absence of surface-active contaminants in the aqueous phase. The viscosity and density of the aqueous phase is relevant in interfacial shear rheology experiments, where the obtained shear stress needs to be corrected with respect to the bulk drag as discussed above [104]. An overview of relevant metadata for the aqueous phase in interface science experiments is provided in Table 11.

2.3.2. Gaseous phase

Most experiments performed at the liquid-gas interface are performed with aqueous solutions in contact with ambient air. In this case, information regarding the chemical composition and pressure of the gas phase is implicit and does generally not require further specification. If specialized gas mixtures are used, however, it is important to state the composition, pressure, and flow rate of the gas phase, as it can affect the adsorption of surface-active species. Particularly alkane vapors can condense at fluid interfaces and compete with other adsorbed species [158,321,322]. The gas composition and pressure affect γ of the pure gas-water interface [323,324], and a reduced γ can result in a decreased adsorption of surface-active species [325]. The use of inert gases can be of benefit for the study of surface-active species that are prone to oxidation, such as phospholipids or oleic acid [326,327]. At increased gas pressure, the gas molecules also increasingly accumulate at the interface and compete with the adsorption of surface-active species [37], particularly for CO_2, which can form clathrate complexes with water at the interface [328]. An overview of relevant metadata for the gaseous phase in interface science experiments is provided in Table 12.

2.3.3. Oil phase

The oil subphase affects the adsorption via the interactions between oil molecules and the adsorbed surface-active species. Furthermore, the hydrophobicity (inverse polarity) of the oil phase determines γ_{ow}, and thus the thermodynamic driving force for adsorption. The γ_{ow} of the clean o/w interface is a good measure for the hydrophobicity of the used oil, with hydrophobic oils exhibiting a higher γ_{ow} [80]. For surfactants, the interfacial competition with short-chained or polar oils can reduce

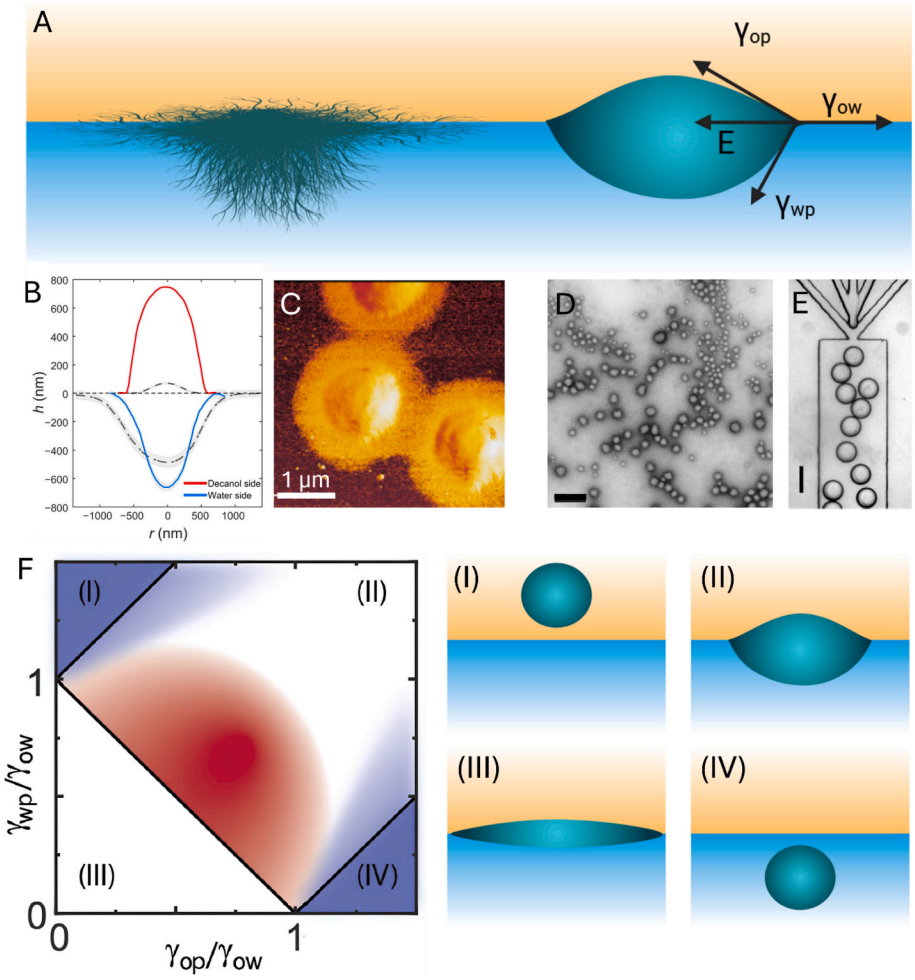


Fig. 6. A) Schematic of synthetic microgels adopting a 'fried-egg' morphology (left) and biopolymeric microgels adopting a lenticular shape based on particle wetting, interfacial stresses, and particle elasticity at fluid interfaces. B) Average height profile of pNIPAM microgels at oil/water interface for hydrophobic hexadecane (black dotted lines) and polar decanol (colored lines). Reprinted from Vialetto et al. (Ref. 121. C) AFM phase image of pNIPAM microgels transferred from the o/w interface onto a solid substrate. Reprinted with permission from Scheidegger et al. (Ref. 290. D) β-lactoglobulin microgels formed by heat-aggregation at 85 °C and pH 5.8. Scale bar corresponds to 0.5 μm. Reprinted with permission from Schmitt et al. (Ref. 291. E) Microfluidic formation of agarose-gelatin composite microgels. Scale bar corresponds to 250 μm. Reprinted with permission by Chau et al. (Ref. 292 F) Prediction of perfectly soft particle positioning and spreading at a fluid interface depending on wetting and interfacial tension. I) Spherical particle in oil phase, II) particle adsorbs and deforms at the interface, III) particle completely spreads in the interfacial plane, IV) spherical particle in aqueous phase. Adapted from Style et al. (Ref. 288. Created in BioRender. Bertsch, P. (2026) https://BioRender.com/8ocrqgn.

their interfacial coverage, while the co-solubility of polar oils in water or and the interfacial layer decreases the CMC of charged surfactants [36,41,44,131,158,329,330]. For proteins, more hydrophobic oils result in a higher surface coverage and can lead to increased intramolecular rearrangements due to the higher surface stresses [31,331–334]. The adsorption of particles is inherently determined by particle wetting which is determined by γ_{ow} and γ_{so} (**Fig. 5A**, **B**, and **I**) [251–253]. For charged nanoparticles, ε_r further determines long-range Coulombic repulsion between particles through the oil phase [256]. Some oils can interact chemically with the surface-active species, e.g., the aldehyde group of octanal that interacts with amino groups of proteins, and can lead to extraordinarily high surface loads [31]. Oils rich in triglycerides undergo slow autohydrolysis that is accelerated at high pH or by reactive oxygen species, so that surface-active fatty acids and monoglycerides can be released that interfere with interfacial experiments [335,336]. Similar to the aqueous phase, great care is required not to introduce surface-active contaminants via the oil phase that may affect interfacial experiments. Oils may contain polar contaminants which can interfere with interfacial experiments and require purification using magnesium silicate, or ideally, column chromatography prior to experiments [80,123,337]. Again, a measurement of the clean oil-water interfacial tension γ_{ow} over the same timescale as adsorption experiments is good practice to confirm the absence of surface-active contaminants. An overview of relevant metadata for the oil phase in interface science experiments is provided in Table 13.

3. The 'Interface Science Data Repository'

We have defined the relevant data of common fluid interface science experiments, as well as metadata of relevant methods, surface-active species and subphases. The relevant metadata is figuratively summarized in Fig. 7. To foster the Findability, Accessibility, Interoperability, and Reusability of interface science data, we establish the Interface Science Data Repository (zenodo.org/communities/isdr) for the sharing of fluid interface science data and metadata. Furthermore, templates for specific interface science experiments, surface-active species, and subphases are provided (zenodo.org/records/19680999) to enhance the uniformity of data format. The different templates can be combined as individual building blocks for interface science experiments, reporting: i) all relevant data of the technique used, ii) relevant metadata for

Table 10
Overview of relevant metadata for microgels in interface science experiments.

Data	Unit	Equation	Comment
Microgels metadata			
Concentration C	kg/L	–	–
Polymerization procedure	–	–	Report used monomer(s), crosslinker and protocol used (e.g. batch vs semi-batch [290,297,298] Report purification protocol [306]
Microgel size	m	–	Include information on dispersity and swelling behavior [121]
Microgel shape/ structure	–	–	Report internal density profile [121,302] Report structure for core-shell or anisotropic microgels in case of polymerization around inorganic core [299–302]
Microgel stiffness	N/m	–	Often tuned qualitatively via crosslinking density [121]
Volume phase transition temperature VPTT	K	–	32°C for pNIPAM microgels [296,303]
ζ-potential (pH, I)	V	–	–
Biopolymeric microgels (additional considerations)			
Used biopolymer and microgel formation procedure	–	–	Report details for in-house microgel production and characterizaion [241]

Table 11
Overview of relevant metadata for the aqueous phase in interface science experiments.

Data	Unit	Equation	Comment
Aqueous phase metadata			
Temperature	°C, K	–	Report means of temperature control
pH	–	$pH = -log[H^+]$	Determines charge of charged and particularly amphoteric surface-active species
Ionic strength I	mol/L	$I = \frac{1}{2}\sum_{i=1}^{n} c_i z_i^2$	Relevant for ionic charge screening
Buffer salts	–	–	May affect surfactants [319,320] and proteins [317,318] due to lyotropic effects
Clean air-water surface tension γ_{aw}	N/m	–	Relevant to detect surface-active contaminations in the aqueous phase (clean a/w surface $\gamma_{aw} \approx 72.4$ mN/m, oils see below)
Viscosity	Pa•s	–	Relevant for interfacial shear rheology correction [99,100,104]
Density	kg/L	–	Relevant for interfacial shear rheology correction [99,100,104] and tensiometry methods relying on drop shape (density difference) [82,83]

surface-active species, and iii) metadata for subphases. An example based on a recent dataset [338] is provided (zenodo.org/records/19680554). Uploading a dataset on Zenodo creates a persistent identifier, i.e., DOI, that can be linked bidirectionally to published articles. A further integral part of FAIR data reporting is the use of standardized and open formats that allow interoperability and reuse across disciplines, systems, and time. In practice, this means sharing of data in tabular form (instead of as PDF or images), avoiding export files from specialized or paid software, using standard and unambiguous vocabulary and units, as well as providing all information on software or code used for data processing [63].

For the time being, making data available requires considerable human efforts for data curation and uploading, while the readability and interoperability of spreadsheets is limited for machines. An outlook on

Table 12
Overview of relevant metadata for the gaseous phase in interface science experiments.

Data	Unit	Equation	Comment
Gaseous phase metadata			
Temperature	°C, K	–	Report means of temperature control
Gas composition	–	–	Implicit for air Report potential interactions with aqueous phase [37,328]
Gas pressure (+ flow rate when continuous gas flushing is used)	N/m²	–	Implicit for air Report potential interactions with aqueous phase [37,328]
Viscosity	Pa•s	–	Relevant for interfacial shear rheology correction [99,100,104]
Density	kg/L	–	Relevant for interfacial shear rheology correction [99,100,104] and tensiometry methods relying on drop shape (density difference) [82,83]

Table 13
Overview of relevant metadata for the oil phase in interface science experiments.

Data	Unit	Equation	Comment
Oil phase metadata			
Temperature	°C, K	–	Report means of temperature control
Name & molecular structure	–	–	Report purity and composition or purification protocol [80]
Clean oil-water interfacial tension γ_{ow}	N/m	–	Relevant to detect surface-active contaminations in the aqueous and oil phase. Good measure for oil polarity (more polar oils have lower γ_{ow}) [80]
Aqueous solubility	mol/L	–	More aqueous soluble oils can act as co-solvents of surface-active species and affect their behavior in solution or adsorption [41]
Relative permittivity ε_r	–	–	Determines electrostatic repulsion through the oil phase [256,257]
Viscosity	Pa•s	–	Relevant for interfacial shear rheology correction [99,100,104]
Density	kg/L	–	Relevant for interfacial shear rheology correction [99,100,104] and tensiometry methods relying on drop shape (density difference) [82,83]

future developments, including automated machine-readable (meta) data conversion, is given below. While we aimed for a universal definition of (meta)data, the diversity of fluid interface science disciplines is large. Some of our proposed (meta)data may not be important in all fields and applications of interface science, while others may appear underrepresented in specialized fields. Our framework and templates might thus not be applicable to all experiments, and users are encouraged to modify and upload adapted versions.

The definition of relevant data and metadata, data reporting templates, and the Interface Science Data Repository should greatly facilitate the FAIRness of fluid interface science data. We consider this a first step towards an increased culture of FAIR data sharing and reuse in interface science that can be actively and continuously advanced towards machine-actionable and AI-assisted scientific data infrastructures. We call upon the interface science community to put our initial proposition for data sharing into practice, and together establish, and nourish, a more FAIR data environment.

4. Outlook

4.1. Towards automated and machine-operable databases

The Interface Science Data Repository presented here is intended as a

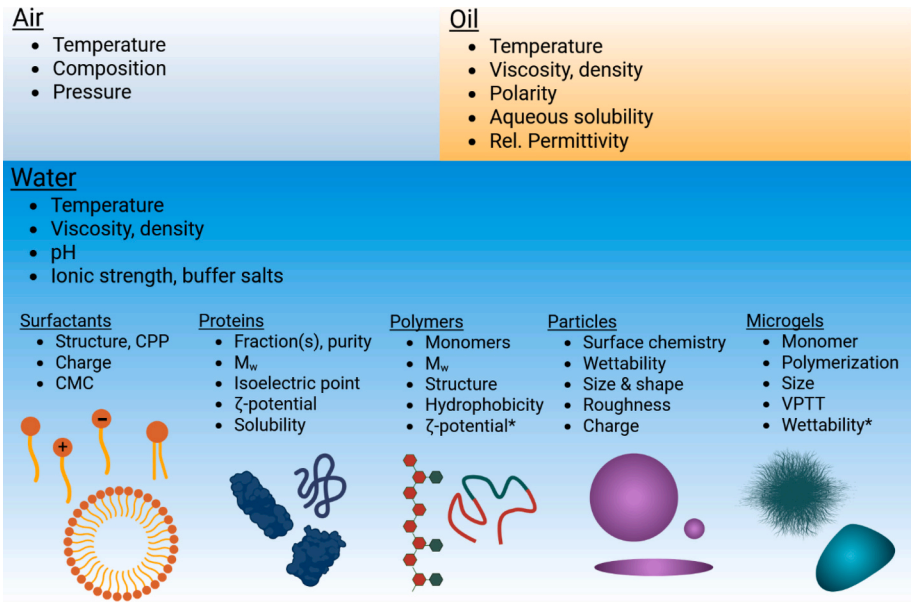


Fig. 7. Overview of relevant metadata for surface-active species and subphases for interface science experiments. Asterisks* indicate additional considerations for surface-active polysaccharides (polymers) and biopolymeric microgels. Created in BioRender. Bertsch, P. (2026) https://BioRender.com/8q91yz2.

first step towards FAIR data sharing in experimental interface science. At present, the repository relies on community-driven manual deposition of experimental data and metadata in a general-purpose repository. Zenodo provides an accessible, sustainable, and widely adopted platform for initiating community-wide data sharing. However, it is not intended to provide advanced semantic data management, automated data processing or knowledge discovery. Yet, it provides an important foundation for the development of (meta)data schema and automated data processing pipelines to enable scaling of the Interface Science Data Repository. For highly heterogeneous research fields such as interface science, establishing community consensus on which experimental (meta)data should be reported and a centralized data repository is a necessary prerequisite before more sophisticated automated data infrastructures can be developed [66,339]. This allows assembling a range of data sources and an overview of available (meta)data formats present in the current data corpus.

To move from this primarily human-operated repository towards a machine-operable database (Fig. 8), a priority will be the automation of converting human-readable (meta)data files to machine-readable metadata. While spreadsheets currently provide an accessible exchange format, future implementations could provide standardized pipelines for conversions to machine-readable representations such as JSON-LD, JSON Schema, YAML, RO-Crate, or FAIR Digital Objects. Such representations would facilitate automated validation of deposited datasets, improve interoperability between repositories, and enable computational workflows to directly interpret experimental metadata without manual intervention [62,63,340,341]. Automated analysis pipelines provide an executable record of the operations performed on data (such as unit conversions, column renaming, and calculations). As such, they can be inspected for correctness and re-run in response to changes in the source data or in data-processing requirements [50,342,343]. The large diversity of interface science instruments and their manufacturers will likely impair a fast transition to standardized machine-readable metadata files. While instrument and subphase metadata can likely be readily integrated in instrument setups, automated metadata recording for surface-active species will be challenging due to their structural and physicochemical complexity discussed above.

Establishing semantic data models is a further important step to improve interoperability. The development of ontologies and controlled vocabularies for interface science would allow experimental variables, materials, measurement methods, and processing steps to be described using standardized terminology. These semantic annotations could support knowledge graphs linking related experiments across laboratories, allowing researchers to identify datasets based on scientific concepts rather than only keyword searches [344,345]. The establishment of controlled vocabularies may pose a challenge in interface science, as exemplified, e.g., by the term ‘elasticity’, that may refer to several phenomena within interface science as well as many other scientific disciplines. Therefore, building ontologies is as much a scientific consensus exercise as a technical one.

The combination of standardized metadata and semantic annotations would enable more sophisticated data discovery methods. Rather than relying solely on conventional metadata filtering, future repositories could incorporate semantic search, vector embeddings, and recommendation algorithms to identify scientifically related experiments based on experimental conditions, material compositions, or measurement outcomes. This allows for large-scale meta-analyses and accelerated hypothesis generation across previously disconnected datasets [344,346,347]. Interface science datasets are often relatively small and generated under widely varying physicochemical conditions using chemically complex surface-active species. Here, artificial intelligence could assist during data deposition and quality control (QC) by identifying missing metadata, detecting inconsistencies between reported experimental parameters, estimating confidence scores for metadata completeness, or recommending related datasets [348–350]. Relational databases queried using Structured Query Language (SQL) can provide a standardized framework for organizing interfacial data [50]. These technologies enable data models to be defined and structured concisely, facilitating efficient filtering and retrieval through the use of queries. In this respect, we foresee large language models being of great value. Such models can be provided with the database schema and a user's question in natural language, which can then be translated into an SQL query to extract the data required by the researcher.

An important direction will be the automation of metadata extraction and improved interoperability directly between instruments and repositories. Most interface science experiments already produce extensive digital records, including instrument settings, acquisition parameters, raw measurement files, lab notebooks, and data processing protocols. Software tools could automatically extract relevant metadata directly from these sources [73,341,351,352], reducing manual curation

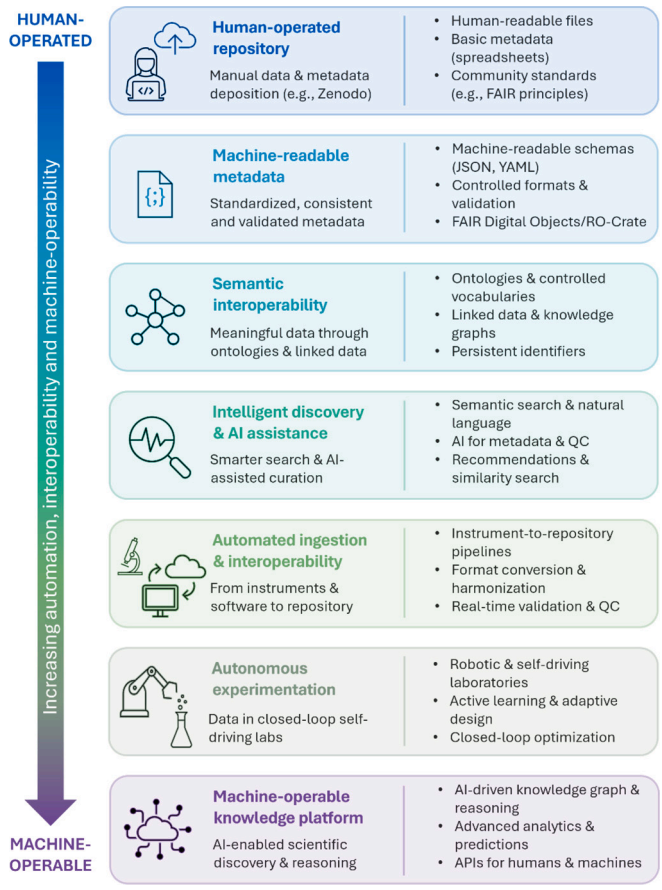


Fig. 8. Roadmap from human-operated repository to automated machine-operable interface science database.

and improving consistency and completeness of deposited records. However, tools for automated metadata extraction are often highly method- or even file-specific [352], while interface science encompasses numerous commercial and custom-built instruments with proprietary file formats. The overlap of relevant metadata across different interface science methods could facilitate metadata extraction across methods, while the diversity of methods and surface-active species again poses some potential challenges. Development of open conversion tools and standardized export interfaces would enable automatic transformation of heterogeneous instrument outputs into uniform metadata formats suitable for repository deposition [353,354]. Such interoperability will likely require collaboration between instrument manufacturers, software developers, and the scientific community. We envisage that large language models could be of great use in rapidly prototyping the range of scripts required for these conversions, for example by providing the source file and a schema of the desired structured target format.

Standardized machine-operable data infrastructures would enable integration with autonomous experimentation platforms. Increasingly, automated laboratories and closed-loop optimization systems combine automated experimentation with machine learning [71]. Although such systems are currently scarce in interface science [154], standardized metadata schemas and interoperable repositories would provide an important foundation for future autonomous experimental workflows. As mentioned above, direct conversion from instrument vendor formats would greatly facilitate interfacing, e.g., the Interface Science Data Repository, with self-driving laboratories.

Ultimately, the combination of standardized metadata, semantic interoperability, automated data ingestion, and AI-assisted curation could enable the development of fully machine-operable interface science knowledge platforms. Rather than functioning solely as repositories for storing datasets, such platforms can integrate heterogeneous experimental data into interconnected knowledge graphs that capture relationships between materials, experimental conditions, and measurement techniques. These structured knowledge representations could support advanced analytics and enable reasoning across previously unrelated studies. Through standardized application programming interfaces (APIs), these knowledge platforms could become directly accessible to both human researchers and computational workflows, allowing seamless integration into modelling environments, digital twins, and autonomous experimentation platforms.

The framework presented here should therefore be viewed as the first stage of a broader evolution from human-curated data sharing towards increasingly machine-actionable and AI-assisted scientific data infrastructures (Fig. 8).

4.2. *Considerations for the development of neural network models*

The provision of aggregated, high-quality and diverse data offered by the Interface Data Science Repository will also be essential to the development of advanced models for interfacial property prediction. Machine learning, particularly neural network-based modelling, has become a powerful and accessible approach for developing quantitative structure-property relationship (QSPR) models that map molecular or biomolecular structure onto interfacial properties. This rise in popularity is driven in part by the growing availability of technologies and frameworks for programming and training neural networks, enabling researchers to construct models capable of processing diverse data structures such as molecular graphs, amino acid sequences, and grid-based representations of materials. A range of neural network architectures have been applied within interface science of small molecules, including multilayer perceptrons [355–357] and message-passing graph neural networks [49,358–361]. The flexibility of graph neural networks allows system components to be encoded in a variety of ways. For example, graphs can be used to represent molecules, sequences for proteins, or grids for materials such as metal-organic frameworks. In addition to their modelling capabilities, neural network methods increasingly support explainable AI techniques that map prediction outcomes back onto input structures, aiding interpretability. Such approaches remain at an early stage within interface science, although work on interpretability has been reported for adsorption at solid surfaces [362]. Neural network models are thus well suited to the development of models which account for the diversity of components in interfacial systems. However, their development is strongly dependent on the provision of large, good quality, information-rich datasets which contain enough information to train and validate them, stressing the need for increased sharing of data and rich metadata in interface science. Furthermore, model development between research groups requires that teams have access to similar data for benchmarking. Such data should be readily available and prepared via a provenance-preserving, transparent process, which the Interface Science Data Repository could provide.

When assembling datasets for interfacial property prediction, an essential consideration is the information richness and structural diversity of the collected data. Models trained on datasets containing a wide range of molecular structures are more likely to generalize well to unseen compounds, whereas datasets dominated by repeated measurements of structurally similar molecules may provide only limited benefit for model development. Therefore, targeting the collection of a broad coverage of chemical space is preferable to seeking out replicated measurements if the aim is to target structure-to-property models. Training models on multiple related properties can improve performance, particularly when individual measurements are missing or sparsely reported [363]. Such multiproperty training has been used to model surfactant adsorption isotherms despite incomplete provision of a complete set of properties for the full dataset [49,359]. Whilst this approach may lend limited benefit to the prediction of well-represented

properties such as CMC, it can enhance the predictions of properties with fewer reported values such as Γ_{max}. These examples illustrate that even partially complete databases can be valuable when multiple related properties are available. While the direct correlation of structure and interfacial behavior usually allows reliable predictions for surfactants, amino acid sequence alone often is not a reliable predictor for protein interfacial adsorption, demanding additional considerations particularly in the low-data regime [364,365].

Another consideration is characterization of irreducible noise in experimental data that sets a lower bound on measurable model accuracy [366]. Aggregating data across multiple laboratories can help to quantify both systematic and random errors, thereby enabling clearer assessment of the discernible limits of model performance. Interlaboratory studies remain scarce in interface science [13,367], potentially afflicting model accuracy, and stressing the need for detailed (meta)data reporting.

Database versioning, e.g., via GitHub [49,359,368], ensures reproducibility in modelling activities, contributing to preventing data leakage, and tracking dataset changes during model development. Version control also allows databases to be dynamic so that they can grow and be updated. As discussed above, rigorous data curation and advanced query functions, such as substructure searches and property-based filtering, are critical for database development. Differences in curation strategies have been shown to influence model performance [369], reinforcing the importance of standardized procedures and curation throughout data collection and processing.

Accurate and consistent sample identification and structural representation are essential for model development. Unique identifiers are required to ensure that samples are correctly curated and that duplicate entries can be detected [73,370]. For instance, molecular structures should be given as standardized, machine-readable representations such as InChI strings. SMILES strings are often preferred as structural representations for small molecules. Trivial, systematic, brand, or code names may be included as supplementary identifiers, but they must be accompanied, if possible, by unambiguous structural notations. Decoding these names into structures is laborious and error prone, requiring significant human intervention to ensure structures are reported accurately. In interface science, this may not always be possible due to the structural complexity or inhomogeneity of some surface-active species as discussed above. For models such as graph neural networks, it is important to ensure that small molecule entries include complete atomic and bonding information such as charges, stereochemistry, and hybridization states [49]. These features are frequently used by models and inconsistencies can lead models either to misinterpret structurally similar compounds as distinct or to disregard features altogether. Structural reporting must also account for the diverse nature of interfacial system components such as macromolecules, proteins, and coordination complexes, which cannot all be represented by SMILES strings effectively. Indeed, systems containing an arbitrary number of components must also be possible to represent in a database. Hierarchical data formats such as JSON can be of help in this regard [371,372].

In addition to structural encodings, calculated molecular descriptors can serve as useful features for modelling. Descriptors that are computationally inexpensive can be generated on demand [373,374], whereas more costly quantum chemical or thermodynamic descriptors are often better provided directly within the database to avoid unnecessary repeated calculations, especially when computed using large computational resources or closed source software [375]. Where available, three-dimensional structural information such as X-ray diffraction data or sets of conformers can provide useful information for modelling. For example, the SPICE dataset provides over 1.1 million conformers, targeted at enabling and developing machine learning potentials for a range of molecules and peptides [368]. Three-dimensional data can be reported in a range of standard formats, such as SDF (structure data format), PDB (Protein Data Bank Format), MOL (MolFile), mmCIF (macromolecular Crystallographic Information Framework) or XYZ files.

Experimental conditions are highly important to interfacial properties and must be recorded alongside structural information. Detailed information regarding the measurement method and metadata, as defined above, should be stored in an accessible and standardized format, as they influence both the behavior of chemical systems and the interpretation of reported properties. Including condition factors in models has been performed in some preliminary neural network predictors of interfacial properties [360,361]. However, the limited availability of well annotated datasets makes it difficult to evaluate these models beyond small test sets. In particular, the effects of conditions that alter molecular speciation, such as pH variations, are challenging to model accurately due to insufficient training data. As a result, progress towards condition-aware predictive models is constrained by the lack of comprehensive experimental metadata. Including complete and consistently reported (meta)data and making it available, e.g., via the Interface Science Data Repository, is critical for advancing the development and assessment of more detailed models.

CRediT authorship contribution statement

Pascal Bertsch: Writing – original draft, Visualization, Data curation, Conceptualization. **Emmanouil Chatzigiannakis:** Writing – review & editing. **Peter Fischer:** Writing – review & editing. **Emma Hinderink:** Writing – review & editing. **Lucio Isa:** Writing – review & editing. **Martin Leser:** Writing – review & editing. **Julia Maldonado-Valderrama:** Writing – review & editing. **Reinhard Miller:** Writing – review & editing. **Brent S. Murray:** Writing – review & editing. **William E. Robinson:** Writing – review & editing. **Leonard Sagis:** Writing – review & editing. **Jacopo Vialetto:** Writing – review & editing. **Jack Yang:** Writing – review & editing. **Martin Malmsten:** Writing – review & editing.

Declaration of competing interest

JMV and RM are editors for *Advances in Colloid and Interface Science*. The other authors have no conflict of interest to declare.

Acknowledgements

The authors thank Stefan Salentinig and Jörg Läuger for helpful inputs and Melanie Bamert for assistance with graphical design. EC acknowledges financial support from the FAIR Data Fund Grant 2023, funded by the 4TU ResearchData (the Netherlands) and from the Replication Studies Research Program (https://doi.org/10.61686/HMOXJ57850), funded by the Dutch Research Council (NWO) (the Netherlands). WER acknowledges funding from the National Growth Fund project “Big Chemistry” (1420578), funded by the Ministry of Education, Culture and Science, the Netherlands.

Data availability

Templates for data upload to the repository and examples are available on Zenodo

References

[1] Nel AE, Mädler L, Velegol D, Xia T, Hoek EMVV, Somasundaran P, et al. Understanding biophysicochemical interactions at the Nano-bio interface. Nat Mater 2009;8(7):543–57. https://doi.org/10.1038/nmat2442.
[2] Hermans E, Saad Bhamla M, Kao P, Fuller GG, Vermant J. Lung surfactants and different contributions to thin film stability. Soft Matter 2015;11(41):8048–57. https://doi.org/10.1039/c5sm01603g.
[3] Castner DG, Ratner BD. Biomedical Surface Science: Foundations to FrontiersVol. 500; 2002. https://doi.org/10.1016/S0039-6028(01)01587-4.
[4] Bertsch P, Bergfreund J, Windhab EJ, Fischer P. Physiological fluid interfaces: functional microenvironments, drug delivery targets, and first line of defense. Acta Biomater 2021;130:32–53. https://doi.org/10.1016/j.actbio.2021.05.051.

[5] Torcello-Gómez A, Maldonado-Valderrama J, Martín-Rodríguez A, McClements DJ. Physicochemical properties and digestibility of emulsified lipids in simulated intestinal fluids: influence of interfacial characteristics. Soft Matter 2011;7(13):6167–77. https://doi.org/10.1039/c1sm05322a.
[6] Maldonado-Valderrama J. Probing in vitro digestion at oil–water interfaces. Curr Opin Colloid Interface Sci 2019;39:51–60. https://doi.org/10.1016/j.cocis.2019.01.004.
[7] Reis P, Holmberg K, Watzke H, Leser ME, Miller R. Lipases at interfaces: a review. Adv Colloid Interf Sci 2009;147:237–50. https://doi.org/10.1016/j.cis.2008.06.001.
[8] Rühs PA, Bergfreund J, Bertsch P, Gstöhl SJ, Fischer P. Complex fluids in animal survival strategies. Soft Matter 2021;17(11):3022–36. https://doi.org/10.1039/D1SM00142F.
[9] Cooper A, Kennedy MW. Biofoams and natural protein surfactants. Biophys Chem 2010;151(3):96–104. https://doi.org/10.1016/j.bpc.2010.06.006.
[10] Wessels JGH. Fungal hydrophobins: proteins that function at an interface. Trends Plant Sci 1996;1(1):9–15. https://doi.org/10.1016/S1360-1385(96)80017-3.
[11] Yang J, Plankensteiner L, de Groot A, Hennebelle M, Sagis LMC, Nikiforidis CV. The role of oleosins and phosphatidylcholines on the membrane mechanics of oleosomes. J Colloid Interface Sci 2025;678:1001–11. https://doi.org/10.1016/j.jcis.2024.09.171.
[12] Liu X, Duncan JH. The effects of surfactants on spilling breaking waves. Nature 2003;421(6922):520–3. https://doi.org/10.1038/nature01357.
[13] Rickard PC, Uher G, Upstill-Goddard RC, Frka S, Mustaffa NIH, Banko-Kubis HM, et al. Reconsideration of seawater surfactant activity analysis based on an inter-laboratory comparison study. Mar Chem 2019;208:103–11. https://doi.org/10.1016/j.marchem.2018.11.012.
[14] Bergfreund J, Wobill C, Evers FM, Hohermuth B, Bertsch P, Lebreton L, et al. Impact of microplastic pollution on breaking waves. Phys Fluids 2024;36(7):072108. https://doi.org/10.1063/5.0208507.
[15] Collins-Gold LC, Lyons RT, Bartholow LC. Parenteral emulsions for drug delivery. Adv Drug Deliv Rev 1990;5(3):189–208. https://doi.org/10.1016/0169-409X(90)90016-L.
[16] Marti-Mestres G, Nielloud F. Emulsions in health care applications—an overview. J Dispers Sci Technol 2002;23(1–3):419–39. https://doi.org/10.1080/01932690208984214.
[17] Malmsten M. Soft drug delivery systems. Soft Matter 2006;2(9):760. https://doi.org/10.1039/b608348j.
[18] Luengo GS, Leonforte F, Greaves A, Rubio RG, Guzman E. Physico-chemical challenges on the self-assembly of natural and bio-based ingredients on hair surfaces: towards sustainable haircare formulations. Green Chem 2023;25(20):7863–82. https://doi.org/10.1039/D3GC02763E.
[19] Luengo GS, Guzman E, Fernández-Peña L, Leonforte F, Ortega F, Rubio RG. Interaction of polyelectrolytes and surfactants on hair surfaces. deposits and their characterization. In: Surface Science and Adhesion in Cosmetics. Wiley; 2021. p. 401–49. https://doi.org/10.1002/9781119654926.ch13.
[20] Murray BS. Interfacial rheology of food emulsifiers and proteins. Curr Opin Colloid Interface Sci 2002;7(5–6):426–31. https://doi.org/10.1016/S1359-0294(02)00077-8.
[21] Berton-Carabin CC, Sagis L, Schroën K. Formation, structure, and functionality of interfacial layers in food emulsions. Annu Rev Food Sci Technol 2018;9(1):551–87. https://doi.org/10.1146/annurev-food-030117-012405.
[22] Berton-Carabin C, Schroën K. Towards new food emulsions: designing the interface and beyond. Curr Opin Food Sci 2019;27:74–81. https://doi.org/10.1016/j.cofs.2019.06.006.
[23] Chatzigiannakis E, Alicke A, Bars L, Le Bidoire L, Vermant J. The hidden subtlety of beer foam stability: a blueprint for advanced foam formulations. Phys Fluids 2025;37(8). https://doi.org/10.1063/5.0274943.
[24] Wei P, Luo Q, Edgehouse KJ, Hemmingsen CM, Rodier BJ, Pentzer EB. 2D particles at fluid-fluid interfaces: assembly and templating of hybrid structures for advanced applications. ACS Appl Mater Interfaces 2018;10(26):21765–81. https://doi.org/10.1021/acsami.8b07178.
[25] Kummer N, Huguenin-Elie L, Zeller A, Chandorkar Y, Schoeller J, Zuber F, et al. 2D foam film coating of antimicrobial lysozyme amyloid fibrils onto cellulose nanopapers. Nanoscale Adv 2023;5(19):5276–85. https://doi.org/10.1039/D3NA00370A.
[26] Freer EM, Yim KS, Fuller GG, Radke CJ. Shear and dilatational relaxation mechanisms of globular and flexible proteins at the hexadecane/water interface. Langmuir 2004;20(23):10159–67. https://doi.org/10.1021/la0485226.
[27] Arooj M, Gandhi NS, Kreck CA, Arrigan DWM, Mancera RL. Adsorption and unfolding of lysozyme at a polarized aqueous–organic liquid interface. J Phys Chem B 2016;120(12):3100–12. https://doi.org/10.1021/acs.jpcb.6b00536.
[28] Tiffany J. The normal tear film. Dev Ophthalmol 2008;41:1–20. https://doi.org/10.1159/000131066.
[29] Zhao Q, Ding L, Xia M, Huang X, Isobe K, Handa A, et al. Role of lysozyme on liquid egg white foaming properties: Interface behavior, physicochemical characteristics and protein structure. Food Hydrocoll 2021;120:106876. https://doi.org/10.1016/j.foodhyd.2021.106876.
[30] Mitropoulos V, Mütze A, Fischer P. Mechanical properties of protein adsorption layers at the air/water and oil/water interface: a comparison in light of the thermodynamical stability of proteins. Adv Colloid Interf Sci 2014;206:195–206. https://doi.org/10.1016/j.cis.2013.11.004.
[31] Bergfreund J, Bertsch P, Fischer P. Adsorption of proteins to fluid interfaces: role of the hydrophobic subphase. J Colloid Interface Sci 2021;584:411–7. https://doi.org/10.1016/j.jcis.2020.09.118.
[32] Lin L, Bergfreund J, Fischer P, Bertsch P. Plant protein adsorption at oil–water interfaces: a mapping review using alternate subphase tensiometry. Curr Opin Colloid Interface Sci 2025;77:101920. https://doi.org/10.1016/j.cocis.2025.101920.
[33] Guzman RZ, Carbonell RG, Kilpatrick PK. The adsorption of proteins to gas-liquid interfaces. J Colloid Interface Sci 1986;114(2):536–47. https://doi.org/10.1016/0021-9797(86)90439-X.
[34] Fainerman VB, Lucassen-Reynders EH. Adsorption of single and mixed ionic surfactants at fluid interfaces. Adv Colloid Interf Sci 2002;96(1–3):295–323. https://doi.org/10.1016/S0001-8686(01)00086-0.
[35] Gurkov TD, Dimitrova DT, Marinova KG, Bilke-Crause C, Gerber C, Ivanov IB. Ionic surfactants on fluid interfaces: determination of the adsorption; role of the salt and the type of the hydrophobic phase. Colloids Surfaces A Physicochem Eng Asp 2005;261(1–3):29–38. https://doi.org/10.1016/j.colsurfa.2004.11.040.
[36] Pradines V, Fainerman VB, Aksenenko EV, Krägel J, Mucic N, Miller R. Adsorption of alkyl trimethylammonium bromides at the water/air and water/hexane interfaces. Colloids Surfaces A Physicochem Eng Asp 2010;371(1–3):22–8. https://doi.org/10.1016/j.colsurfa.2010.08.052.
[37] Miller R, Aksenenko EV, Fainerman VB. Dynamic interfacial tension of surfactant solutions. Adv Colloid Interf Sci 2017;247:115–29. https://doi.org/10.1016/j.cis.2016.12.007.
[38] Eastoe J, Dalton JS. Dynamic surface tension and adsorption mechanisms of surfactants at the air–water interface. Adv Colloid Interf Sci 2000;85(2–3):103–44. https://doi.org/10.1016/S0001-8686(99)00017-2.
[39] Borwankar RP, Wasan DT. Equilibrium and dynamics of adsorption of surfactants at fluid-fluid interfaces. Chem Eng Sci 1988;43(6):1323–37. https://doi.org/10.1016/0009-2509(88)85106-6.
[40] Deshiikan SR, Bush D, Eschenazi E, Papadopoulos KD. SDS, brij58 and CTAB at the Dodecane-water interface. Colloids Surfaces A Physicochem Eng Asp 1998;136(1–2):133–50. https://doi.org/10.1016/S0927-7757(97)00323-3.
[41] Bergfreund J, Siegenthaler S, Lutz-Bueno V, Bertsch P, Fischer P. Surfactant adsorption to different fluid interfaces. Langmuir 2021;37(22):6722–7. https://doi.org/10.1021/acs.langmuir.1c00668.
[42] Fainerman VB, Miller R, Möhwald H. General relationships of the adsorption behavior of surfactants at the water/air interface. J Phys Chem B 2002;106(4):809–19. https://doi.org/10.1021/jp012672x.
[43] Sloutskin E, Tamam L, Sapir Z, Ocko BM, Bain CD, Kuzmenko I, et al. Counterions under a surface-adsorbed cationic surfactant monolayer: structure and thermodynamics. Langmuir 2022;38(40):12356–66. https://doi.org/10.1021/acs.langmuir.2c02076.
[44] Rehfeld SJ. Adsorption of sodium dodecyl sulfate at various hydrocarbon-water interfaces. J Phys Chem 1967;71(3):738–45. https://doi.org/10.1021/j100862a039.
[45] Oliveira EB, Correia EL, Winter HH, Razavi S. Scaling dynamics of particles confined at fluid–fluid interfaces. Soft Matter 2026;22(20):3620–32. https://doi.org/10.1039/D6SM00118A.
[46] Kotsmar C, Pradines V, Alahverdjieva VS, Aksenenko EV, Fainerman VB, Kovalchuk VI, et al. Thermodynamics, adsorption kinetics and rheology of mixed protein–surfactant interfacial layers. Adv Colloid Interf Sci 2009;150(1):41–54. https://doi.org/10.1016/j.cis.2009.05.002.
[47] Noskov BA, Krycki MM. Formation of protein/surfactant adsorption layer as studied by dilational surface rheology. Adv Colloid Interf Sci 2017;247:81–99. https://doi.org/10.1016/j.cis.2017.07.003.
[48] Dan A, Gochev G, Krägel J, Aksenenko EV, Fainerman VB, Miller R. Interfacial rheology of mixed layers of food proteins and surfactants. Curr Opin Colloid Interface Sci 2013;18(4):302–10. https://doi.org/10.1016/j.cocis.2013.04.002.
[49] Hödl SL, Hermans L, Dankloff PFJ, Piruska A, Huck WTS, Robinson WE. SurfPro – a curated database and predictive model of experimental properties of surfactants. Dig Dis 2025;4(5):1176–87. https://doi.org/10.1039/D4DD00393D.
[50] Hödl SL, Dankloff PFJ, Korotkevich AA, Huck WTS, Robinson WE. SurfPro2: a relational database, curation workflow and repository of surfactant physicochemical data. ChemRxiv 2026. https://doi.org/10.26434/chemrxiv.15006392/v1.
[51] Sudol PE, Cramer JA, Hinnant KM, Brown LC, Snow AW, Bunton CM, et al. Investigating correlations between physical properties and fire suppression performance of fluorinated and fluorine-free foams using a novel firefighting foam database. Colloids Surfaces A Physicochem Eng Asp 2023;679:132533. https://doi.org/10.1016/j.colsurfa.2023.132533.
[52] Cramer JA, Bunton CM, Davis MC, Sudol PE, Hinnant KM, Snow AW, et al. Predicting the firefighting efficacy of surfactants prior to synthesis via ensemble artificial neural network modeling of a foam performance database. J Surfactant Deterg 2025;28(5):1009–29. https://doi.org/10.1002/jsde.12849.
[53] Hinnant KM, Sudol PE, Cramer JA, Moore DW, Brown LC, Bunton CM, et al. Database of surfactant structure and properties to aid in the development of fluorine-free, fire-suppressing surfactants and foams. ACS Omega 2025;10(37):42270–81. https://doi.org/10.1021/acsomega.5c01726.
[54] Wang H, Chen J, Liu W, Wang D, Song Y, Hong H, et al. Using machine learning for green substitution of industrial chemicals: integrating functionality, hazard, and life cycle impact. Chem Rev 2026;126(2):841–94. https://doi.org/10.1021/acs.chemrev.5c00828.
[55] Tenopir C, Dalton ED, Allard S, Frame M, Pjesivac I, Birch B, et al. Changes in data sharing and data reuse practices and perceptions among scientists worldwide. PLoS One 2015;10(8):e0134826. https://doi.org/10.1371/journal.pone.0134826.
[56] Tenopir C, Rice NM, Allard S, Baird L, Borycz J, Christian L, et al. Data sharing, management, use, and reuse: practices and perceptions of scientists worldwide.

PLoS One 2020;15(3):e0229003. https://doi.org/10.1371/journal.pone.0229003.
[57] Khan N, Thelwall M, Kousha K. Data sharing and reuse practices: disciplinary differences and improvements needed. Online Inf Rev 2023;47(6):1036–64. https://doi.org/10.1108/OIR-08-2021-0423.
[58] Piwowar HA, Day RS, Fridsma DB. Sharing detailed research data is associated with increased citation rate. PLoS One 2007;2(3):e308. https://doi.org/10.1371/journal.pone.0000308.
[59] Christensen G, Dafoe A, Miguel E, Moore DA, Rose AK. A study of the impact of data sharing on article citations using journal policies as a natural experiment. PLoS One 2019;14(12):e0225883. https://doi.org/10.1371/journal.pone.0225883.
[60] Colavizza G, Cadwallader L, LaFlamme M, Dozot G, Lecorney S, Rappo D, et al. An analysis of the effects of sharing research data, code, and preprints on citations. PLoS One 2024;19(10):e0311493. https://doi.org/10.1371/journal.pone.0311493.
[61] Groth P, Cousijn H, Clark T, Goble C. FAIR data reuse – the path through data citation. Data Intell 2020;2(1–2):78–86. https://doi.org/10.1162/dint_a_00030.
[62] Radha SK, Kuehlkamp A, Nabrzyski J. Advancing transparency and responsibility in machine learning: the critical role of FAIR principles - a comprehensive review. ACM J Respons Comput 2025;2(4):1–38. https://doi.org/10.1145/3768151.
[63] Wilkinson MD, Dumontier M, Aalbersberg LJJ, Appleton G, Axton M, Baak A, et al. The FAIR guiding principles for scientific data management and stewardship. Sci Data 2016;3(1):160018. https://doi.org/10.1038/sdata.2016.18.
[64] Foster ED, Deardorff A. Open science framework (OSF). J Med Libr Assoc 2017;105(2):38. https://doi.org/10.5195/jmla.2017.88.
[65] Ramachandran R, Bugbee K, Murphy K. From open data to open science. Earth Sp Sci 2021;8(5):e2020EA001562. https://doi.org/10.1029/2020EA001562.
[66] Sicilia M-A, García-Barriocanal E, Sánchez-Alonso S. Community curation in open dataset repositories: insights from zenodo. Procedia Comput Sci 2017;106:54–60. https://doi.org/10.1016/j.procs.2017.03.009.
[67] Scheffler M, Aeschlimann M, Albrecht M, Bereau T, Bungartz H-J, Felser C, et al. FAIR data enabling new horizons for materials research. Nature 2022;604(7907):635–42. https://doi.org/10.1038/s41586-022-04501-x.
[68] Benson DA, Cavanaugh M, Clark K, Karsch-Mizrachi I, Ostell J, Pruitt KD, et al. GenBank. Nucleic Acids Res 2018;46:D41–7. https://doi.org/10.1093/nar/gkx1094.
[69] Berman H, Henrick K, Nakamura H. Announcing the worldwide protein data bank. Nat Struct Mol Biol 2003;10(12):980. https://doi.org/10.1038/nsb1203-980.
[70] Wenger M, Ochsenbein F, Egret D, Dubois P, Bonnarel F, Borde S, et al. The SIMBAD astronomical database. Astron Astrophys Suppl Ser 2000;143(1):9–22. https://doi.org/10.1051/aas:2000332.
[71] Pendleton IM, Cattabriga G, Li Z, Najeeb MA, Friedler SA, Norquist AJ, et al. Experiment specification, capture and laboratory automation technology (ESCALATE): a software pipeline for automated chemical experimentation and data management. MRS Commun 2019;9(3):846–59. https://doi.org/10.1557/mrc.2019.72.
[72] Stracke K, Evans JD. The rise of data repositories in materials chemistry. Commun Chem 2024;7(1):63. https://doi.org/10.1038/s42004-024-01143-0.
[73] Archibald M, Bruno I, Chalk S, Davies AN, Hanson RM, Kuhn S, et al. FAIRSpec-ready spectroscopic data collections – advice for researchers, authors, and data managers (IUPAC technical report). Pure Appl Chem 2025;97(11):1479–510. https://doi.org/10.1515/pac-2025-0409.
[74] Steinbeck C, Koepler O, Bach F, Herres-Pawlis S, Jung N, Liermann J, et al. NFDI4Chem - towards a national research data infrastructure for chemistry in Germany. Res Ideas Outcomes 2020;6:1–100. https://doi.org/10.3897/rio.6.e55852.
[75] Maldonado-Valderrama J, Fainerman VB, Aksenenko E, Jose Gálvez-Ruiz M, Cabrerizo-Vílchez MA, Miller R. Dynamics of protein adsorption at the oil–water interface: comparison with a theoretical model. Colloids Surfaces A Physicochem Eng Asp 2005;261(1–3):85–92. https://doi.org/10.1016/j.colsurfa.2004.10.131.
[76] Bergfreund J, Sun Q, Fischer P, Bertsch P. Adsorption of charged anisotropic nanoparticles at oil-water interfaces. Nanoscale Adv 2019;1(11):4308–12. https://doi.org/10.1039/C9NA00506D.
[77] Foo KY, Hameed BH. Insights into the modeling of adsorption isotherm systems. Chem Eng J 2010;156(1):2–10. https://doi.org/10.1016/j.cej.2009.09.013.
[78] Mukherjee I, Moulik SP, Rakshit AK. Tensiometric determination of gibbs surface excess and micelle point: a critical revisit. J Colloid Interface Sci 2013;394(1):329–36. https://doi.org/10.1016/j.jcis.2012.12.004.
[79] Du K, Glogowski E, Emrick T, Russell TP, Dinsmore AD. Adsorption energy of nano- and microparticles at liquid-liquid interfaces. Langmuir 2010;26(15):12518–22. https://doi.org/10.1021/la100497h.
[80] Bergfreund J, Bertsch P, Fischer P. Effect of the hydrophobic phase on interfacial phenomena of surfactants, proteins, and particles at fluid interfaces. Curr Opin Colloid Interface Sci 2021;56:101509. https://doi.org/10.1016/j.cocis.2021.101509.
[81] El Mahrab-Robert M, Rosilio V, Bolzinger M, Chaminade P, Grossiord J. Assessment of oil polarity: comparison of evaluation methods. Int J Pharm 2008;348(1–2):89–94. https://doi.org/10.1016/j.ijpharm.2007.07.027.
[82] Berry JD, Neeson MJ, Dagastine RR, Chan DYC, Tabor RF. Measurement of surface and interfacial tension using pendant drop tensiometry. J Colloid Interface Sci 2015;454:226–37. https://doi.org/10.1016/j.jcis.2015.05.012.
[83] Nagel M, Tervoort TA, Vermant J. From drop-shape analysis to stress-fitting elastometry. Adv Colloid Interf Sci 2017;247:33–51. https://doi.org/10.1016/j.cis.2017.07.008.
[84] Sudheesh S, Ahmad J. Effect of wilhelmy plate material on hysteresis of langmuir film isotherms. Asian J Chem 2013;25(7):3535–8. https://doi.org/10.14233/ajchem.2013.13213.
[85] Wu N, Dai J, Micale FJ. Dynamic surface tension measurement with a dynamic wilhelmy plate technique. J Colloid Interface Sci 1999;215(2):258–69. https://doi.org/10.1006/jcis.1999.6270.
[86] Rodríguez-Hakim M, Jaensson N, Vermant J. Towards operating windows for pendant drop methods: Tensiometry and rheometry of elastic interfaces. Rheol Acta 2025;64(9–10):461–81. https://doi.org/10.1007/s00397-025-01493-z.
[87] Petkov JT, Gurkov TD, Campbell BE, Borwankar RP. Dilatational and shear elasticity of gel-like protein layers on air/water interface. Langmuir 2000;16(8):3703–11. https://doi.org/10.1021/la991287k.
[88] Verwijlen T, Imperiali L, Vermant J. Separating viscoelastic and compressibility contributions in pressure-area isotherm measurements. Adv Colloid Interf Sci 2014;206:428–36. https://doi.org/10.1016/j.cis.2013.09.005.
[89] Jaensson N, Vermant J. Tensiometry and rheology of complex interfaces. Curr Opin Colloid Interface Sci 2018;37:136–50. https://doi.org/10.1016/j.cocis.2018.09.005.
[90] Erni P. Deformation modes of complex fluid interfaces. Soft Matter 2011;7(17):7586–600. https://doi.org/10.1039/c1sm05263b.
[91] Duncan SL, Larson RG. Comparing experimental and simulated pressure-area isotherms for DPPC. Biophys J 2008;94(8):2965–86. https://doi.org/10.1529/biophysj.107.114215.
[92] Sagis LMC, Liu B, Li Y, Essers J, Yang J, Moghimikheirabadi A, et al. Dynamic heterogeneity in complex interfaces of soft Interface-dominated materials. Sci Rep 2019;9(1):2938. https://doi.org/10.1038/s41598-019-39761-7.
[93] Sagis LMC, Fischer P. Nonlinear rheology of complex fluid-fluid interfaces. Curr Opin Colloid Interface Sci 2014;19(6):520–9. https://doi.org/10.1016/j.cocis.2014.09.003.
[94] Risse K, Yang J, de Groot A, Giménez-Ribes G, Shen P, Drusch S, et al. Advances in large amplitude oscillatory dilatational surface rheology – a review. Adv Colloid Interf Sci 2025;345:103625. https://doi.org/10.1016/j.cis.2025.103625.
[95] Rühs PA, Scheuble N, Windhab EJ, Fischer P. Protein adsorption and interfacial rheology interfering in dilatational experiment. Eur Phys J Spec Top 2013;222(1):47–60. https://doi.org/10.1140/epjst/e2013-01825-0.
[96] Murray BS, Cattin B, Schüler E, Sonmez ZO. Response of adsorbed protein films to rapid expansion. Langmuir 2002;18(24):9476–84. https://doi.org/10.1021/la026050u.
[97] Fuller GG, Vermant J. Complex fluid-fluid interfaces: rheology and structure. Annu Rev Chem Biomol Eng 2012;3(1):519–43. https://doi.org/10.1146/annurev-chembioeng-061010-114202.
[98] Birbaum FC, Haavisto S, Koponen A, Windhab EJ, Fischer P. Shear localisation in interfacial particle layers and its influence on Lissajous-plots. Rheol Acta 2016;55(4):267–78. https://doi.org/10.1007/s00397-016-0912-0.
[99] Edwards DA, Brenner H, Wasan DT. Interfacial transport processes and rheology. Butterworth-Heinemann; 1991.
[100] Sánchez-Puga P, Tajuelo J, Pastor JM, Rubio MA. BiconeDrag—A data processing application for the oscillating conical bob interfacial shear rheometer. Comput Phys Commun 2019;239:184–96. https://doi.org/10.1016/j.cpc.2019.01.020.
[101] Verwijlen T, Moldenaers P, Stone HA, Vermant J. Study of the flow field in the magnetic rod interfacial stress rheometer. Langmuir 2011;27(15):9345–58. https://doi.org/10.1021/la201109u.
[102] Tajuelo J, Pastor JM, Martínez-Pedrero F, Vázquez M, Ortega F, Rubio RG, et al. Magnetic microwire probes for the magnetic rod interfacial stress rheometer. Langmuir 2015;31(4):1410–20. https://doi.org/10.1021/la5038316.
[103] Zell ZA, Nowbahar A, Mansard V, Leal LG, Deshmukh SS, Mecca JM, et al. Surface shear inviscidity of soluble surfactants. Proc Natl Acad Sci 2014;111(10):3677–82. https://doi.org/10.1073/pnas.1315991111.
[104] Renggli D, Alicke A, Ewoldt RH, Vermant J. Operating windows for oscillatory interfacial shear rheology. J Rheol 2020;64(1):141–60. https://doi.org/10.1122/1.5130620.
[105] Vandebril S, Franck A, Fuller GG, Moldenaers P, Vermant J. A double wall-ring geometry for interfacial shear rheometry. Rheol Acta 2010;49(2):131–44. https://doi.org/10.1007/s00397-009-0407-3.
[106] Erni P, Fischer P, Windhab EJ, Kusnezov V, Stettin H, Läuger J. Stress- and strain-controlled measurements of interfacial shear viscosity and viscoelasticity at liquid/liquid and gas/liquid interfaces. Rev Sci Instrum 2003;74(11):4916–24. https://doi.org/10.1063/1.1614433.
[107] Tajuelo J, Rubio MA, Pastor JM. Flow field based data processing for the oscillating conical bob interfacial shear rheometer. J Rheol 2018;62(1):295–311. https://doi.org/10.1122/1.5012764.
[108] Sánchez-Puga P, Tajuelo J, Pastor J, Rubio M. Dynamic measurements with the bicone interfacial shear rheometer: numerical bench-marking of flow field-based data processing. Colloids Interfaces 2018;2(4):69. https://doi.org/10.3390/colloids2040069.
[109] Kralchevsky PA, Denkov ND, Paunov VN, Velev OD, Ivanov IB, Yoshimura H, et al. Formation of two-dimensional colloid crystals in liquid films under the action of capillary forces. J Phys Condens Matter 1994;6(23A):395–402.
[110] Madivala B, Fransaer J, Vermant J. Self-assembly and rheology of ellipsoidal particles at interfaces. Langmuir 2009;25(5):2718–28. https://doi.org/10.1021/la803554u.

[111] Choi SQ, Steltenkamp S, Zasadzinski JA, Squires TM. Active microrheology and simultaneous visualization of sheared phospholipid monolayers. Nat Commun 2011;2(1):312. https://doi.org/10.1038/ncomms1321.
[112] Hoenig D, Moebius D. Direct visualization of monolayers at the air-water interface by Brewster angle microscopy. J Phys Chem 1991;95(12):4590–2. https://doi.org/10.1021/j100165a003.
[113] Hénon S, Meunier J. Microscope at the Brewster angle: direct observation of first-order phase transitions in monolayers. Rev Sci Instrum 1991;62(4):936–9. https://doi.org/10.1063/1.1142032.
[114] Makai L, Kalas B, Tiborcz G. Spectroscopic ellipsometry investigation of free liquid-liquid and liquid-air interfaces. Thin Solid Films 2023;764:139634. https://doi.org/10.1016/j.tsf.2022.139634.
[115] Muñoz MG, Monroy F, Ortega F, Rubio RG, Langevin D. Monolayers of symmetric triblock copolymers at the air−water interface. 1. Equilibrium properties. Langmuir 2000;16(3):1083–93. https://doi.org/10.1021/la990142a.
[116] Schlossman ML. Liquid–liquid interfaces: studied by X-ray and neutron scattering. Curr Opin Colloid Interface Sci 2002;7(3–4):235–43. https://doi.org/10.1016/S1359-0294(02)00053-5.
[117] Delcea M, Helm CA. X-ray and neutron reflectometry of thin films at liquid interfaces. Langmuir 2019;35(26):8519–30. https://doi.org/10.1021/acs.langmuir.8b04315.
[118] Atkinson PJ, Dickinson E, Horne DS, Richardson RM. Neutron reflectivity of adsorbed β-casein and β-Lactoglobulin at the air/water interface. J Chem Soc Faraday Trans 1995;91(17):2847–54. https://doi.org/10.1039/FT9959102847.
[119] Kovalchuk MV, Boikova AS, Dyakova YA, Marchenkova MA, Opolchentsev AM, Pisarevsky YV, et al. Modification of the langmuir–schaefer method for fabrication of ordered protein films. Crystallogr Reports 2017;62(4):632–8. https://doi.org/10.1134/S1063774517040125.
[120] Wu X, Yuan Q, Liu S, Shi S, Russell TP, Wang D. Nanorod-surfactant assemblies and their interfacial behavior at liquid-liquid interfaces. ACS Macro Lett 2019;8:512–8. https://doi.org/10.1021/acsmacrolett.9b00134.
[121] Vialetto J, Ramakrishna SN, Isa L. In situ imaging of the three-dimensional shape of soft responsive particles at fluid interfaces by atomic force microscopy. Sci Adv 2022;8(45):32–5. https://doi.org/10.1126/sciadv.abq2019.
[122] Reguera J, Ponomarev E, Geue T, Stellacci F, Bresme F, Moglianetti M. Contact angle and adsorption energies of nanoparticles at the air-liquid interface determined by neutron reflectivity and molecular dynamics. Nanoscale 2015;7(13):5665–73. https://doi.org/10.1039/C5NR00620A.
[123] Paunov VN. Novel method for determining the three-phase contact angle of colloid particles adsorbed at air−water and oil−water interfaces. Langmuir 2003;19(19):7970–6. https://doi.org/10.1021/la0347509.
[124] Isa L, Lucas F, Wepf R, Reimhult E. Measuring single-nanoparticle wetting properties by freeze-fracture shadow-casting Cryo-scanning electron microscopy. Nat Commun 2011;2(1):438. https://doi.org/10.1038/ncomms1441.
[125] Murphy BM, Götz A, Gutt C, McGuinness C, Rønnow HM, Schneidewind A, et al. FAIR data – the photon and neutron communities move together towards open science. IUCrJ 2025;12(1):8–15. https://doi.org/10.1107/S2052252524011941.
[126] Lee RM, Eisenman LR, Khuon S, Aaron JS, Chew T-L. Believing is seeing – the deceptive influence of bias in quantitative microscopy. J Cell Sci 2024;137(1):1–10. https://doi.org/10.1242/jcs.261567.
[127] Linkert M, Rueden CT, Allan C, Burel J-M, Moore W, Patterson A, et al. Metadata matters: access to image data in the real world. J Cell Biol 2010;189(5):777–82. https://doi.org/10.1083/jcb.201004104.
[128] Nagarajan R. Molecular packing parameter and surfactant self-assembly: the neglected role of the surfactant tail. Langmuir 2002;18(1):31–8. https://doi.org/10.1021/la010831y.
[129] Lutz-Bueno V, Isabettini S, Walker F, Kuster S, Liebi M, Fischer P. Ionic micelles and aromatic additives: a closer look at the molecular packing parameter. Phys Chem Chem Phys 2017;19(32):21869–77. https://doi.org/10.1039/C7CP03891G.
[130] Freire RVM, Salentinig S. Amphiphilic lipids for food functionality. Curr Opin Colloid Interface Sci 2024;72:101817. https://doi.org/10.1016/j.cocis.2024.101817.
[131] Peltonen L, Hirvonen J, Yliruusi J. The behavior of sorbitan surfactants at the water–oil interface: straight-chained hydrocarbons from pentane to dodecane as an oil phase. J Colloid Interface Sci 2001;240(1):272–6. https://doi.org/10.1006/jcis.2001.7612.
[132] Ennis J. Spontaneous curvature of surfactant films. J Chem Phys 1992;97(1):663–78. https://doi.org/10.1063/1.463561.
[133] Shinoda K, Arai H. The correlation between phase inversion temperature in emulsion and cloud point in solution of nonionic emulsifier. J Phys Chem 1964;68(12):3485–90. https://doi.org/10.1246/nikkashi1948.87.8_818.
[134] Israelachvili, J. N.; Mitchell, D. J.; Ninham, B. W. Theory of self-assembly of hydrocarbon amphiphiles into micelles and bilayers. j. Chem. Soc. Faraday Trans *2* 1976, 72, 1525. doi:https://doi.org/10.1039/f29767201525.
[135] Winsor PA. Hydrotropy, solubilisation and related emulsification processes. Trans Faraday Soc 1948;44:376. https://doi.org/10.1039/tf9484400376.
[136] Salager J, Marquez N, Graciaa A, Lachaise J. Partitioning of ethoxylated octylphenol surfactants in microemulsion−oil−water systems: influence of temperature and relation between partitioning coefficient and physicochemical formulation. Langmuir 2000;16(13):5534–9. https://doi.org/10.1021/la9905517.
[137] Kunz W, Testard F, Zemb T. Correspondence between curvature, packing parameter, and hydrophilic−lipophilic deviation scales around the phase-inversion temperature. Langmuir 2009;25(1):112–5. https://doi.org/10.1021/la8028879.
[138] Salager J, Graciaa A, Marquez R. Analyzing the surfactant classification confusion through the HLD formulation equation. JCIS Open 2022;8:100060. https://doi.org/10.1016/j.jciso.2022.100060.
[139] Witthayapanyanon A, Harwell JH, Sabatini DA. Hydrophilic–Lipophilic Deviation (HLD) method for characterizing conventional and extended surfactants. J Colloid Interface Sci 2008;325(1):259–66. https://doi.org/10.1016/j.jcis.2008.05.061.
[140] Griffin WC. Classification of surface-active agents by“ HLB”. J Soc Cosmet Chem 1949;1(5):311–26.
[141] Pasquali RC, Taurozzi MP, Bregni C. Some considerations about the hydrophilic–lipophilic balance system. Int J Pharm 2008;356(1–2):44–51. https://doi.org/10.1016/j.ijpharm.2007.12.034.
[142] Kharazi M, Saien J, Miller R. The surface activity of surfactants at liquid interfaces: the role of CMC, decrease in surface tension, HLB, thermodynamic adsorption models. J Surfactant Deterg 2026;29(1):65–90. https://doi.org/10.1002/jsde.12902.
[143] Pisaev IV, Soboleva OA, Ivanova NI. Adsorption of brij 35-Dodecylpyridinium bromide mixtures at air-aqueous solution and Teflon-aqueous solution interfaces. Colloid J 2009;71(2):246–51. https://doi.org/10.1134/S1061933X09020148.
[144] Okuda H, Ozeki S, Ikeda S. The adsorption of dodecyldimethylammonium bromide on aqueous surfaces of sodium bromide solutions. Bull Chem Soc Jpn 1984;57(5):1321–7. https://doi.org/10.1246/bcsj.57.1321.
[145] Nakamura A, Tajima K, Sasaki T. The effect of the PH on the adsorption of an ampholytic surfactant, N-dodecyl-β-alanine, at the aqueous surface. Bull Chem Soc Jpn 1975;48(1):214–8. https://doi.org/10.1246/bcsj.48.214.
[146] Manne S, Warr GG. Supramolecular structure of surfactants confined to interfaces. ACS Symp Ser 1999;736:2–23. https://doi.org/10.1021/bk-1999-0736.ch001.
[147] Bergendal E, Gutfreund P, Pilkington GA, Campbell RA, Müller-Buschbaum P, Holt SA, et al. Tuneable interfacial surfactant aggregates mimic lyotropic phases and facilitate large scale nanopatterning. Nanoscale 2021;13(1):371–9. https://doi.org/10.1039/D0NR06621D.
[148] Lin S-Y, Lin Y-Y, Chen E-M, Hsu C-T, Kwan C-C. A study of the equilibrium surface tension and the critical micelle concentration of mixed surfactant solutions. Langmuir 1999;15(13):4370–6. https://doi.org/10.1021/la981149f.
[149] Pitt AR, Morley SD, Burbidge NJ, Quickenden EL. The relationship between surfactant structure and limiting values of surface tension, in aqueous gelatin solution, with particular regard to multilayer coating. Colloids Surfaces A Physicochem Eng Asp 1996;114:321–35. https://doi.org/10.1016/0927-7757(96)03593-5.
[150] Czajka A, Hazell G, Eastoe J. Surfactants at the design limit. Langmuir 2015;31(30):8205–17. https://doi.org/10.1021/acs.langmuir.5b00336.
[151] Lu JR, Thomas RK, Penfold J. Surfactant layers at the air/water interface: structure and composition. Adv Colloid Interf Sci 2000;84(1–3):143–304. https://doi.org/10.1016/S0001-8686(99)00019-6.
[152] Sato R, Tsukagoshi S, Tanaka L, Arai N. Tail unsaturation controls monoglyceride monolayer organization and oil–water interfacial tension. Chem Phys 2026;607:113167. https://doi.org/10.1016/j.chemphys.2026.113167.
[153] Premadasa UI, Ma Y-Z, Sacci RL, Bocharova V, Thiele NA, Doughty B. Understanding self-assembly and the stabilization of liquid/liquid interfaces: the importance of ligand tail branching and oil-phase solvation. J Colloid Interface Sci 2022;609:807–14. https://doi.org/10.1016/j.jcis.2021.11.088.
[154] Dankloff PFJ, van Rossum M, Baltussen MG, Hödl SL, ten Klooster DHW, van de Voort E, et al. An autonomous robotic module for efficient surface tension measurements of formulations. npj Comput Mater 2025;11(1):358. https://doi.org/10.1038/s41524-025-01842-9.
[155] Eastoe J, Nave S, Downer A, Paul A, Rankin A, Tribe K, et al. Adsorption of ionic surfactants at the air−solution interface. Langmuir 2000;16(10):4511–8. https://doi.org/10.1021/la991564n.
[156] Martínez-Balbuena L, Arteaga-Jiménez A, Hernández-Zapata E, Márquez-Beltrán C. Applicability of the Gibbs adsorption isotherm to the analysis of experimental surface-tension data for ionic and nonionic surfactants. Adv Colloid Interf Sci 2017;247:178–84. https://doi.org/10.1016/j.cis.2017.07.018.
[157] Langmuir I. The constitution and fundamental properties of solids and liquids. Part II. Liquids. J Am Chem Soc 1917;39:1828–907.
[158] Fainerman VB, Aksenenko EV, Kovalchuk VI, Mucic N, Javadi A, Liggieri L, et al. New view of the adsorption of surfactants at water/alkane interfaces – competitive and cooperative effects of surfactant and alkane molecules. Adv Colloid Interf Sci 2020;279:102143. https://doi.org/10.1016/j.cis.2020.102143.
[159] Cockbain EG. The adsorption of sodium dodecyl sulphate at the oil-water interface and application of the gibbs equation. Trans Faraday Soc 1954;50(3):874. https://doi.org/10.1039/tf9545000874.
[160] Jiang Z, Li X, Yang G, Cheng L, Cai B, Yang Y, et al. PH-responsive surface activity and solubilization with novel Pyrrolidone-based gemini surfactants. Langmuir 2012;28(18):7174–81. https://doi.org/10.1021/la3008156.
[161] Ferri JK, Stebe KJ. Which surfactants reduce surface tension faster? A scaling argument for diffusion-controlled adsorption. Adv Colloid Interf Sci 2000;85(1):61–97. https://doi.org/10.1016/S0001-8686(99)00027-5.
[162] Bonfillon A, Sicoli F, Langevin D. Dynamic surface tension of ionic surfactant solutions. J Colloid Interface Sci 1994;168(2):497–504. https://doi.org/10.1006/jcis.1994.1447.
[163] Haydon DA, Phillips JN. The gibbs equation and the surface equation of state for soluble ionized monolayers in absence of added electrolyte at the oil-water interface. Trans Faraday Soc 1958;54(4):698. https://doi.org/10.1039/tf9585400698.
[164] MacRitchie F. Protein adsorption/desorption at fluid interfaces. Colloids Surf A Physicochem Eng Asp 1989;41:25–34. https://doi.org/10.1016/0166-6622(89)80038-1.

[165] Beverung CJ, Radke CJ, Blanch HW. Protein adsorption at the oil/water interface: characterization of adsorption kinetics by dynamic interfacial tension measurements. Biophys Chem 1999;81(1):59–80. https://doi.org/10.1016/S0301-4622(99)00082-4.
[166] Dickinson E, Matsumura Y. Proteins at liquid interfaces: role of the molten globule state. Colloids Surf B: Biointerfaces 1994;3(1–2):1–17. https://doi.org/10.1016/0927-7765(93)01116-9.
[167] Miller R, Grigoriev D, Krägel J, Makievski A, Maldonado-Valderrama J, Leser M, et al. Experimental studies on the desorption of adsorbed proteins from liquid interfaces. Food Hydrocoll 2005;19(3):479–83. https://doi.org/10.1016/j.foodhyd.2004.10.012.
[168] Malmsten M. Formation of adsorbed protein layers. J Colloid Interface Sci 1998;207(2):186–99. https://doi.org/10.1006/jcis.1998.5763.
[169] van der Veen M, Stuart MC, Norde W. Spreading of proteins and its effect on adsorption and desorption kinetics. Colloids Surf B: Biointerfaces 2007;54(2):136–42. https://doi.org/10.1016/j.colsurfb.2006.08.017.
[170] Benjamins J, De Feijter JA, Evans MTA, Graham DE, Phillips MC. Dynamic and static properties of proteins adsorbed at the air water interface. Faraday Discuss Chem Soc 1975;59:218–29. https://doi.org/10.1039/DC9755900218.
[171] Olsmats E, Rennie AR. Pea protein [pisum sativum] as stabilizer for oil/water emulsions. Adv Colloid Interf Sci 2024;326:103123. https://doi.org/10.1016/j.cis.2024.103123.
[172] Jarpa-Parra M. Lentil protein: a review of functional properties and food application. An overview of lentil protein functionality. Int J Food Sci Technol 2018;53(4):892–903. https://doi.org/10.1111/ijfs.13685.
[173] Yang J, Sagis LMC. Interfacial behavior of plant proteins — novel sources and extraction methods. Curr Opin Colloid Interface Sci 2021;56:101499. https://doi.org/10.1016/j.cocis.2021.101499.
[174] Bertsch P, Böcker L, Mathys A, Fischer P. Proteins from microalgae for the stabilization of fluid interfaces, emulsions, and foams. Trends Food Sci Technol 2021;108:326–42. https://doi.org/10.1016/j.tifs.2020.12.014.
[175] Yang J, Kornet R, Ntone E, Meijers MGJ, van den Hoek IAF, Sagis LMC, et al. Plant protein aggregates induced by extraction and fractionation processes: impact on techno-functional properties. Food Hydrocoll 2024;155:110223. https://doi.org/10.1016/j.foodhyd.2024.110223.
[176] Issaq HJ, Conrads TP, Janini GM, Veenstra TD. Methods for fractionation, separation and profiling of proteins and peptides. Electrophoresis 2002;23(17):3048–61. https://doi.org/10.1002/1522-2683(200209)23:17<3048::AID-ELPS3048>3.0.CO;2-L.
[177] Bertsch P, Thoma A, Bergfreund J, Geue T, Fischer P. Transient measurement and structure analysis of protein-polysaccharide multilayers at fluid interfaces. Soft Matter 2019;15(31):6362–8. https://doi.org/10.1039/C9SM01112A.
[178] Tang Q, Roos YH, Miao S. Plant protein versus dairy proteins: a PH-dependency investigation on their structure and functional properties. Foods 2023;12(2):368. https://doi.org/10.3390/foods12020368.
[179] Kubiak-Ossowska K, Cwieka M, Kaczynska A, Jachimska B, Mulheran PA. Lysozyme adsorption at a silica surface using simulation and experiment: effects of PH on protein layer structure. Phys Chem Chem Phys 2015;17(37):24070–7. https://doi.org/10.1039/C5CP03910J.
[180] Böcker L, Bertsch P, Wenner D, Teixeira S, Bergfreund J, Eder S, et al. Effect of arthrospira platensis microalgae protein purification on emulsification mechanism and efficiency. J Colloid Interface Sci 2021;584:344–53. https://doi.org/10.1016/j.jcis.2020.09.067.
[181] Ulaganathan V, Retzlaff I, Won JY, Gochev G, Gehin-Delval C, Leser M, et al. B-Lactoglobulin adsorption layers at the water/air surface: 1. Adsorption kinetics and surface pressure isotherm: effect of PH and ionic strength. Colloids Surfaces A Physicochem Eng Asp 2017;519:153–60. https://doi.org/10.1016/j.colsurfa.2016.03.008.
[182] Graham DE, Phillips MC. Proteins at liquid interfaces: I. Kinetics of adsorption and surface denaturation. J Colloid Interface Sci 1979;70(3):403–14. https://doi.org/10.1016/0021-9797(79)90048-1.
[183] Graham D, Phillips M. Proteins at liquid interfaces: II. Adsorption isotherms. J Colloid Interface Sci 1979;70(3):415–26. https://doi.org/10.1016/0021-9797(79)90049-3.
[184] Graham D, Phillips M. Proteins at liquid interfaces: III. Molecular structures of adsorbed films. J Colloid Interface Sci 1979;70(3):427–39. https://doi.org/10.1016/0021-9797(79)90050-X.
[185] Freer EM, Yim KS, Fuller GG, Radke CJ. Interfacial rheology of globular and flexible proteins at the hexadecane/water interface: comparison of shear and dilatation deformation. J Phys Chem B 2004;108(12):3835–44. https://doi.org/10.1021/jp037236k.
[186] Erni P, Windhab EJ, Fischer P. Emulsion drops with complex interfaces: globular versus flexible proteins. Macromol Mater Eng 2011;296(3–4):249–62. https://doi.org/10.1002/mame.201000290.
[187] Miller R, Aksenenko EV, Fainerman VB, Pison U. Kinetics of adsorption of globular proteins at liquid/fluid interfaces. Colloids Surfaces A Physicochem Eng Asp 2001;183–185:381–90. https://doi.org/10.1016/S0927-7757(01)00523-4.
[188] Sengupta T, Damodaran S. Role of dispersion interactions in the adsorption of proteins at oil-water and air-water interfaces. Langmuir 1998;14(22):6457–69. https://doi.org/10.1021/la980275g.
[189] Dalgleish DG. Conformations and structures of milk proteins adsorbed to oil-water interfaces. Food Res Int 1996;29(5–6):541–7. https://doi.org/10.1016/S0963-9969(96)00065-8.
[190] Das KP, Kinsella JE. Effect of heat denaturation on the adsorption of β-Lactoglobulin at the oil/water interface and on coalescence stability of emulsions. J Colloid Interface Sci 1990;139(2):551–60. https://doi.org/10.1016/0021-9797(90)90128-B.
[191] McClellan SJ, Franses EI. Effect of concentration and denaturation on adsorption and surface tension of bovine serum albumin. Colloids Surf B: Biointerfaces 2003;28(1):63–75. https://doi.org/10.1016/S0927-7765(02)00131-5.
[192] Dai L, Bergfreund J, Reichert CL, Fischer P, Weiss J. Shear rheological properties of acid hydrolyzed insoluble proteins from chlorella protothecoides at the oil-water interface. J Colloid Interface Sci 2019;551:297–304. https://doi.org/10.1016/j.jcis.2019.05.029.
[193] Roth S, Murray BS, Dickinson E. Interfacial shear rheology of aged and heat-treated β-Lactoglobulin films: displacement by nonionic surfactant. J Agric Food Chem 2000;48(5):1491–7. https://doi.org/10.1021/jf990976z.
[194] Desfougères Y, Saint-Jalmes A, Salonen A, Vié V, Beaufils S, Pezennec S, et al. Strong improvement of interfacial properties can result from slight structural modifications of proteins: the case of native and dry-heated lysozyme. Langmuir 2011;27(24):14947–57. https://doi.org/10.1021/la203485y.
[195] Ulaganathan V, Retzlaff I, Won JY, Gochev G, Gunes DZ, Gehin-Delval C, et al. B-Lactoglobulin adsorption layers at the water/air surface: 2. Dilational rheology: effect of PH and ionic strength. Colloids Surfaces A Physicochem Eng Asp 2017;521:167–76. https://doi.org/10.1016/j.colsurfa.2016.08.064.
[196] Wierenga PA, Meinders MBJ, Egmond MR, Voragen AGJ, De Jongh HHJ. Quantitative description of the relation between protein net charge and protein adsorption to air-water interfaces. J Phys Chem B 2005;109(35):16946–52. https://doi.org/10.1021/jp050990g.
[197] Rühs PA, Scheuble N, Windhab EJ, Mezzenga R, Fischer P. Simultaneous control of PH and ionic strength during interfacial rheology of β-Lactoglobulin fibrils adsorbed at liquid/liquid interfaces. Langmuir 2012;28(34):12536–43. https://doi.org/10.1021/la3026705.
[198] Malcolm AS, Dexter AF, Middelberg APJ. Mechanical properties of interfacial films formed by lysozyme self-assembly at the air-water interface. Langmuir 2006;22(21):8897–905. https://doi.org/10.1021/la060565u.
[199] Martin AH, Cohen Stuart MA, Bos MA, Van Vliet T. Correlation between mechanical behavior of protein films at the air/water interface and intrinsic stability of protein molecules. Langmuir 2005;21(9):4083–9. https://doi.org/10.1021/la047417t.
[200] Biehn GF, Ernsberger ML. Poly(vinyl alcohol) as an emulsifying agent in vinyl polymerizations. Ind Eng Chem 1948;40(8):1449–53. https://doi.org/10.1021/ie51392a030.
[201] Lochhead RY. The role of polymers in cosmetics: recent trends. In: ACS Symposium Series. 961; 2007. p. 3–56. https://doi.org/10.1021/bk-2007-0961.ch001.
[202] Dijt JC, Cohen Stuart MA, Fleer GJ. Competitive adsorption kinetics of polymers differing in length only. Macromolecules 1994;27(12):3219–28. https://doi.org/10.1021/ma00090a015.
[203] Zhang J, Thomas RK, Penfold J. Collapsed structure of hydrophobically modified polyacrylamide adsorbed at the air–water interface: the polymer surface excess and the Gibbs equation. Langmuir 2020;36(39):11661–75. https://doi.org/10.1021/acs.langmuir.0c02534.
[204] Glass JE. Adsorption characteristics of water-soluble polymers. Poly (vinyl alcohol) and poly (vinylpyrrolidone) at the aqueous-air interface. J Phys Chem 1968;332(17):4450–8.
[205] Lankveld JM, Lyklema J. Adsorption of polyvinyl alcohol on the paraffin—water interface. i. Interfacial tension as a function of time and concentration. J Colloid Interface Sci 1972;41(3):454–65. https://doi.org/10.1016/0021-9797(72)90369-4.
[206] Lankveld JM, Lyklema J. Adsorption of polyvinyl alcohol on the paraffin—water interface. II. Spread and adsorbed monolayers. J Colloid Interface Sci 1972;41(3):466–74. https://doi.org/10.1016/0021-9797(72)90370-0.
[207] Fleer GJ, Stuart MAC, Scheutjens JMHM, Cosgrove T, Vincent B. Polymers at interfaces. Springer Science & Business Media; 1993.
[208] Huggins ML. Solutions of long chain compounds. J Chem Phys 1941;9(5):440. https://doi.org/10.1063/1.1750930.
[209] Flory PJ. Thermodynamics of high polymer solutions. J Chem Phys 1942;10(1):51–61. https://doi.org/10.1063/1.1723621.
[210] de Gennes PG. Polymers at an interface; a simplified view. Adv Colloid Interf Sci 1987;27(3–4):189–209. https://doi.org/10.1016/0001-8686(87)85003-0.
[211] Leclerc E, Daoud M. Multiblock copolymers at interfaces: concentration and selectivity effects. Macromolecules 1997;30(2):293–300. https://doi.org/10.1021/ma960865q.
[212] Aguié-Béghin, V.; Leclerc, E.; Daoud, M.; Douillard, R. Asymmetric Multiblock Copolymers at the Gas–Liquid Interface: Phase Diagram and Surface Pressure. J Colloid Interface Sci 1999, 214 (2), 143–155. doi:https://doi.org/10.1006/jcis.1999.6144.
[213] Blomqvist BR, Wärnheim T, Claesson PM. Surface rheology of PEO−PPO−PEO triblock copolymers at the air−water interface: comparison of spread and adsorbed layers. Langmuir 2005;21(14):6373–84. https://doi.org/10.1021/la0467584.
[214] Ramírez P, Stocco A, Muñoz J, Miller R. Interfacial rheology and conformations of triblock copolymers adsorbed onto the water-oil interface. J Colloid Interface Sci 2012;378(1):135–43. https://doi.org/10.1016/j.jcis.2012.04.033.
[215] Muñoz MG, Monroy F, Ortega F, Rubio RG, Langevin D. Monolayers of symmetric triblock copolymers at the air−water interface. 2. Adsorption kinetics. Langmuir 2000;16(3):1094–101. https://doi.org/10.1021/la9901433.
[216] Kim Y, Pyun J, Fréchet JMJ, Hawker CJ, Frank CW. The dramatic effect of architecture on the self-assembly of block copolymers at interfaces. Langmuir 2005;21(23):10444–58. https://doi.org/10.1021/la047122f.

[217] Stocco, A.; Tauer, K.; Pispas, S.; Sigel, R. Dynamics of amphiphilic diblock copolymers at the air–water interface. J Colloid Interface Sci 2011, 355 (1), 172–178. doi:https://doi.org/10.1016/j.jcis.2010.11.049.
[218] Clifton BJ, Cosgrove T, Richardson RM, Zarbakhsh A, Webster JRP. The structure of block copolymers at the fluid/fluid interface. Phys B Condens Matter 1998;248 (1–4):289–96. https://doi.org/10.1016/S0921-4526(98)00252-X.
[219] Prokop RM, Hair ML, Neumann AW. Interfacial tension of a polystyrene−poly (ethylene oxide) diblock copolymer at the water−toluene interface. Macromolecules 1996;29(18):5902–6. https://doi.org/10.1021/ma960230r.
[220] Gonçalves Da Silva AM, Filipe EJM, D'Oliveira JMR, Martinho JMG. Interfacial behavior of poly(styrene)-poly(ethylene oxide) diblock copolymer monolayers at the air-water interface. Hydrophilic block chain length and temperature influence. Langmuir 1996;12(26):6547–53. https://doi.org/10.1021/la960604+.
[221] Lopes SIC, Gonçalves da Silva AMPS, Brogueira P, Piçarra S, Martinho JMG. Interfacial behavior of poly(isoprene-b-methyl methacrylate) diblock copolymers and their blends with polystyrene at the air−water interface. Langmuir 2007;23 (18):9310–9. https://doi.org/10.1021/la700988s.
[222] Mitra I, Li X, Pesek SL, Makarenko B, Lokitz BS, Uhrig D, et al. Thin film phase behavior of bottlebrush/linear polymer blends. Macromolecules 2014;47(15): 5269–76. https://doi.org/10.1021/ma501070w.
[223] Alaboalirat M, Qi L, Arrington KJ, Qian S, Keum JK, Mei H, et al. Amphiphilic bottlebrush block copolymers: analysis of aqueous self-assembly by small-angle neutron scattering and surface tension measurements. Macromolecules 2019;52 (2):465–76. https://doi.org/10.1021/acs.macromol.8b02366.
[224] Hsieh T-L, Martinez MR, Garoff S, Matyjaszewski K, Tilton RD. Interfacial dilatational rheology as a bridge to connect amphiphilic heterografted bottlebrush copolymer architecture to emulsifying efficiency. J Colloid Interface Sci 2021;581:135–47. https://doi.org/10.1016/j.jcis.2020.07.063.
[225] Seong H-G, Fink Z, Chen Z, Emrick T, Russell TP. Bottlebrush polymers at liquid interfaces: assembly dynamics, mechanical properties, and all-liquid printed constructs. ACS Nano 2023;17(15):14731–41. https://doi.org/10.1021/acsnano.3c02684.
[226] Seong H-G, Jin Z, Chen Z, Hu M, Emrick T, Russell TP. Bottlebrush block copolymers at the interface of immiscible liquids: adsorption and lateral packing. J Am Chem Soc 2024;146(19):13000–9. https://doi.org/10.1021/jacs.3c13817.
[227] Lee K, Gan X, Emrick T, Russell TP. Synthesis of asymmetric bottlebrush random copolymers and their assembly in the bulk and at fluid interfaces. Angew Chem Int Ed 2026;65(19):1–9. https://doi.org/10.1002/anie.2377439.
[228] Erni P, Windhab EJ, Gunde R, Graber M, Pfister B, Parker A, et al. Interfacial rheology of surface-active biopolymers: Acacia Senegal gum versus hydrophobically modified starch. Biomacromolecules 2007;8(11):3458–66. https://doi.org/10.1021/bm700578z.
[229] Niu H, Chen X, Luo T, Chen H, Fu X. The interfacial behavior and long-term stability of emulsions stabilized by gum arabic and sugar beet pectin. Carbohydr Polym 2022;291:119623. https://doi.org/10.1016/j.carbpol.2022.119623.
[230] Bindereif B, Karbstein H, Zahn K, van der Schaaf U. Effect of conformation of sugar beet pectin on the interfacial and emulsifying properties. Foods 2022;11(2): 214. https://doi.org/10.3390/foods11020214.
[231] Li X, Al-Assaf S, Fang Y, Phillips GO. Competitive adsorption between sugar beet pectin (SBP) and hydroxypropyl methylcellulose (HPMC) at the oil/water interface. Carbohydr Polym 2013;91(2):573–80. https://doi.org/10.1016/j.carbpol.2012.08.075.
[232] Atgié M, Chennevière A, Masbernat O, Roger K. Emulsions stabilized by gum arabic: how diversity and interfacial networking lead to metastability. Langmuir 2019;35(45):14553–65. https://doi.org/10.1021/acs.langmuir.9b02541.
[233] Konował E, Sybis M, Prochaska K. Surface activity of hydrophobized modified starch hydrolysates in mixed systems. Materials 2024;17(22):5526. https://doi.org/10.3390/ma17225526.
[234] Desbrières J, López-Gonzalez E, Aguilera-miguel A, Sadtler V, Marchal P, Castel C, et al. Dilational rheology of oil/water interfaces covered by amphiphilic polysaccharides derived from dextran. Carbohydr Polym 2017;177:460–8. https://doi.org/10.1016/j.carbpol.2017.09.011.
[235] Gaonkar AG. Surface and interfacial activities and emulsion characteristics of some food hydrocolloids. Food Hydrocoll 1991;5(4):329–37. https://doi.org/10.1016/S0268-005X(09)80045-3.
[236] Pérez OE, Sánchez CC, Pilosof AMR, Rodríguez Patino JM. Dynamics of adsorption of hydroxypropyl methylcellulose at the air-water interface. Food Hydrocoll 2008;22(3):387–402. https://doi.org/10.1016/j.foodhyd.2006.12.005.
[237] White GW, Katona T, Zodda JP. The use of high-performance size exclusion chromatography (HPSEC) as a molecular weight screening technique for polygalacturonic acid for use in pharmaceutical applications. J Pharm Biomed Anal 1999;20(6):905–12. https://doi.org/10.1016/S0731-7085(99)00083-7.
[238] Gómez-Ordóñez E, Jiménez-Escrig A, Rupérez P. Molecular weight distribution of polysaccharides from edible seaweeds by high-performance size-exclusion chromatography (HPSEC). Talanta 2012;93:153–9. https://doi.org/10.1016/j.talanta.2012.01.067.
[239] Liu D, Tang W, Yin J-Y, Nie S-P, Xie M-Y. Monosaccharide composition analysis of polysaccharides from natural sources: hydrolysis condition and detection method development. Food Hydrocoll 2021;116:106641. https://doi.org/10.1016/j.foodhyd.2021.106641.
[240] Farris S, Mora L, Capretti G, Piergiovanni L. Charge density quantification of polyelectrolyte polysaccharides by conductometric titration: an analytical chemistry experiment. J Chem Educ 2012;89(1):121–4. https://doi.org/10.1021/ed200261w.
[241] Akgonullu DZ, Murray BS, Connell SD, Fang Y, Linter B, Sarkar A. Synthetic and biopolymeric microgels: review of similarities and difference in behaviour in bulk phases and at interfaces. Adv Colloid Interf Sci 2023;320:102983. https://doi.org/10.1016/j.cis.2023.102983.
[242] Aveyard R, Binks BP, Clint JH. Emulsions stabilised solely by colloidal particles. Adv Colloid Interf Sci 2003;100–102:503–46. https://doi.org/10.1016/S0001-8686(02)00069-6.
[243] Stocco A, Rio E, Binks BP, Langevin D. Aqueous foams stabilized solely by particles. Soft Matter 2011;7(4):1260. https://doi.org/10.1039/c0sm01290d.
[244] Binks BP. Colloidal particles at a range of fluid–fluid interfaces. Langmuir 2017; 33(28):6947–63. https://doi.org/10.1021/acs.langmuir.7b00860.
[245] Coertjens S, Moldenaers P, Vermant J, Isa L. Contact angles of microellipsoids at fluid interfaces. Langmuir 2014;30(15):4289–300. https://doi.org/10.1021/la500888u.
[246] Luo AM, Vermant J, Ilg P, Zhang Z, Sagis LMC. Self-assembly of ellipsoidal particles at fluid-fluid interfaces with an empirical pair potential. J Colloid Interface Sci 2019;534:205–14. https://doi.org/10.1016/j.jcis.2018.08.114.
[247] Loudet JC, Alsayed AM, Zhang J, Yodh AG. Capillary interactions between anisotropic colloidal particles. Phys Rev Lett 2005;94(1):018301.
[248] Kutuzov S, He J, Tangirala R, Emrick T, Russell TP, Böker A. On the kinetics of nanoparticle self-assembly at liquid/liquid interfaces. Phys Chem Chem Phys 2007;9(48):6351–8. https://doi.org/10.1039/b710060b.
[249] Maru HC, Wasan DT, Kintner RC. Behavior of a rigid sphere at a liquid—liquid interface. Chem Eng Sci 1971;26(10):1615–28. https://doi.org/10.1016/0009-2509(71)86051-7.
[250] Denkov N, Ivanov I, Kralchevsky P, Wasan D. A possible mechanism of stabilization of emulsions by solid particles. J Colloid Interface Sci 1992;150(2): 589–93. https://doi.org/10.1016/0021-9797(92)90228-E.
[251] Binks BP, Lumsdon SO. Influence of particle wettability on the type and stability of surfactant-free emulsions. Langmuir 2000;16(23):8622–31. https://doi.org/10.1021/la000189s.
[252] Binks BP, Lumsdon SO. Pickering emulsions stabilized by monodisperse latex particles: effects of particle size. Langmuir 2001;17(15):4540–7. https://doi.org/10.1021/la0103822.
[253] Binks BP, Clint JH. Solid wettability from surface energy components: relevance to Pickering emulsions. Langmuir 2002;18(4):1270–3. https://doi.org/10.1021/la011420k.
[254] de Gennes PG. Wetting: statics and dynamics. Rev Mod Phys 1985;57(3):827–63. https://doi.org/10.1103/RevModPhys.57.827.
[255] Paunov VN, Binks BP, Ashby NP. Adsorption of charged colloid particles to charged liquid surfaces. Langmuir 2002;18(18):6946–55. https://doi.org/10.1021/la0203584.
[256] Aveyard R, Clint JH, Nees D, Paunov VN. Compression and structure of monolayers of charged latex particles at air/water and octane/water interfaces. Langmuir 2000;16(4):1969–79. https://doi.org/10.1021/la990887g.
[257] Aveyard R, Binks BP, Clint JH, Fletcher PD, Horozov TS, Neumann B, et al. Measurement of long-range repulsive forces between charged particles at an oil-water interface. Phys Rev Lett 2002;88(24):2461021–4. https://doi.org/10.1103/PhysRevLett.88.246102.
[258] Wang H, Singh V, Behrens SH. Image charge effects on the formation of Pickering emulsions. J Phys Chem Lett 2012;3(20):2986–90. https://doi.org/10.1021/jz300909z.
[259] Marinova KG, Alargova RG, Denkov ND, Velev OD, Petsev DN, Ivanov IB, et al. Charging of oil−water interfaces due to spontaneous adsorption of hydroxyl ions. Langmuir 1996;12(8):2045–51. https://doi.org/10.1021/la950928i.
[260] Roger K, Cabane B. Why are hydrophobic/water interfaces negatively charged? Angew Chem 2012;124(23):5723–6. https://doi.org/10.1002/ange.201108228.
[261] San-Miguel A, Behrens SH. Influence of nanoscale particle roughness on the stability of Pickering emulsions. Langmuir 2012;28(33):12038–43. https://doi.org/10.1021/la302224v.
[262] Zanini M, Marschelke C, Anachkov SE, Marini E, Synytska A, Isa L. Universal emulsion stabilization from the arrested adsorption of rough particles at liquid-liquid interfaces. Nat Commun 2017;8(1):15701. https://doi.org/10.1038/ncomms15701.
[263] Zanini M, Cingolani A, Hsu C-P, Fernández-Rodríguez MÁ, Soligno G, Beltzung A, et al. Mechanical phase inversion of Pickering emulsions via metastable wetting of rough colloids. Soft Matter 2019;15(39):7888–900. https://doi.org/10.1039/C9SM01352K.
[264] Rezvantalab H, Shojaei-Zadeh S. Designing patchy particles for optimum interfacial activity. Phys Chem Chem Phys 2014;16(18):8283. https://doi.org/10.1039/c3cp55512g.
[265] Lehle H, Noruzifar E, Oettel M. Ellipsoidal particles at fluid interfaces. Eur Phys J E 2008;26(1–2):151–60. https://doi.org/10.1140/epje/i2007-10314-1.
[266] Botto L, Yao L, Leheny RL, Stebe KJ. Capillary bond between rod-like particles and the micromechanics of particle-laden interfaces. Soft Matter 2012;8(18): 4971–9. https://doi.org/10.1039/c2sm25211b.
[267] Botto L, Lewandowski EP, Cavallaro M, Stebe KJ. Capillary interactions between anisotropic particles. Soft Matter 2012;8(39):9957–71. https://doi.org/10.1039/c2sm25929j.
[268] Loudet JC, Pouligny B. How do mosquito eggs self-assemble on the water surface? Eur Phys J E 2011;34(8):76. https://doi.org/10.1140/epje/i2011-11076-9.
[269] Hu C, Zhang F, Kong Q, Lu Y, Zhang B, Wu C, et al. Synergistic chemical and photodynamic antimicrobial therapy for enhanced wound healing mediated by multifunctional light- responsive nanoparticles. Biomacromolecules 2019;20: 4581–92. https://doi.org/10.1021/acs.biomac.9b01401.

[270] Cavallaro M, Botto L, Lewandowski EP, Wang M, Stebe KJ. Curvature-driven capillary migration and assembly of rod-like particles. Proc Natl Acad Sci 2011;108(52):20923–8. https://doi.org/10.1073/pnas.1116344108.
[271] Davies GB, Botto L. Dipolar capillary interactions between tilted ellipsoidal particles adsorbed at fluid–fluid interfaces. Soft Matter 2015;11(40):7969–76. https://doi.org/10.1039/C5SM01815C.
[272] Kralchevsky PA, Denkov ND. Capillary forces and structuring in layers of colloid particles. Curr Opin Colloid Interface Sci 2001;6(4):383–401. https://doi.org/10.1016/S1359-0294(01)00105-4.
[273] Paunov VN, Kralchevsky PA, Denkov ND, Nagayama K. Lateral capillary forces between floating submillimeter particles. J Colloid Interface Sci 1993;157(1):100–12. https://doi.org/10.1006/jcis.1993.1163.
[274] Lewandowski EP, Cavallaro M, Botto L, Bernate JC, Garbin V, Stebe KJ. Orientation and self-assembly of cylindrical particles by anisotropic capillary interactions. Langmuir 2010;26(19):15142–54. https://doi.org/10.1021/la1012632.
[275] Aveyard R, Clint JH. New method for the measurement of line tensions at the solid/liquid/air three-phase contact line. J Chem Soc Faraday Trans 1995;91(1):175. https://doi.org/10.1039/ft9959100175.
[276] Faraudo J, Bresme F. Stability of particles adsorbed at liquid/fluid interfaces: shape effects induced by line tension. J Chem Phys 2003;118(14):6518–28. https://doi.org/10.1063/1.1559728.
[277] Hua X, Frechette J, Bevan MA. Nanoparticle adsorption dynamics at fluid interfaces. Soft Matter 2018;14(19):3818–28. https://doi.org/10.1039/C8SM00273H.
[278] Chen H, Jia X, Fairweather M, Hunter TN. Influence of wettability on diffusion limited nanoparticle adsorption at gas-liquid interfaces. JCIS Open 2025;20:100154. https://doi.org/10.1016/j.jciso.2025.100154.
[279] Bizmark N, Ioannidis MA, Henneke DE. Irreversible adsorption-driven assembly of nanoparticles at fluid interfaces revealed by a dynamic surface tension probe. Langmuir 2014;30(3):710–7. https://doi.org/10.1021/la404357j.
[280] Bresme F, Oettel M. Nanoparticles at fluid interfaces. J Phys Condens Matter 2007;19(41):413101.
[281] Lin Y, Skaff H, Emrick T, Dinsmore AD, Russell TP. Nanoparticle assembly and transport at liquid-liquid interfaces. Science 2003;299(5604):226–9. https://doi.org/10.1126/science.1078616.
[282] Bresme F, Faraudo J. Orientational transitions of anisotropic nanoparticles at liquid-liquid interfaces. J Phys Condens Matter 2007;19:375110. https://doi.org/10.1088/0953-8984/19/37/375110.
[283] Gravelle S, Botto L. Adsorption of single and multiple graphene-oxide nanoparticles at a water–vapor interface. Langmuir 2021;37(45):13322–30. https://doi.org/10.1021/acs.langmuir.1c01902.
[284] Reincke F, Hickey SG, Kegel WK, Vanmaekelbergh D. Spontaneous assembly of a monolayer of charged gold nanocrystals at the water/oil interface. Angew Chem Int Ed 2004;43(4):458–62. https://doi.org/10.1002/anie.200352339.
[285] Reincke F, Kegel WK, Zhang H, Nolte M, Wang D, Vanmaekelbergh D, et al. Understanding the self-assembly of charged nanoparticles at the water/oil interface. Phys Chem Chem Phys 2006;8(33):3828–35. https://doi.org/10.1039/B604535A.
[286] Chai Y, Lukito A, Jiang Y, Ashby PD, Russell TP. Fine-tuning nanoparticle packing at water–oil interfaces using ionic strength. Nano Lett 2017;17(10):6453–7. https://doi.org/10.1021/acs.nanolett.7b03462.
[287] Bertsch P, Diener M, Adamcik J, Scheuble N, Geue T, Mezzenga R, et al. Adsorption and interfacial layer structure of unmodified nanocrystalline cellulose at air/water interfaces. Langmuir 2018;34(50):15195–202. https://doi.org/10.1021/acs.langmuir.8b03056.
[288] Style RW, Isa L, Dufresne ER. Adsorption of soft particles at fluid interfaces. Soft Matter 2015;11(37):7412–9. https://doi.org/10.1039/c5sm01743b.
[289] Geisel K, Isa L, Richtering W. Unraveling the 3D localization and deformation of responsive microgels at oil/water interfaces: a step forward in understanding soft emulsion stabilizers. Langmuir 2012;28(45):15770–6. https://doi.org/10.1021/la302974j.
[290] Scheidegger L, Fernández-Rodríguez MÁ, Geisel K, Zanini M, Elnathan R, Richtering W, et al. Compression and deposition of microgel monolayers from fluid interfaces: particle size effects on interface microstructure and nanolithography. Phys Chem Chem Phys 2017;19(13):8671–80. https://doi.org/10.1039/c6cp07896f.
[291] Schmitt C, Bovay C, Vuilliomenet A-M, Rouvet M, Bovetto L, Barbar R, et al. Multiscale characterization of individualized β-Lactoglobulin microgels formed upon heat treatment under narrow PH range conditions. Langmuir 2009;25(14):7899–909. https://doi.org/10.1021/la900501n.
[292] Chau M, Abolhasani M, Thérien-Aubin H, Li Y, Wang Y, Velasco D, et al. Microfluidic generation of composite biopolymer microgels with tunable compositions and mechanical properties. Biomacromolecules 2014;15(7):2419–25. https://doi.org/10.1021/bm5002813.
[293] Zhang J, Pelton R. Poly(N-Isopropylacrylamide) microgels at the air−water interface. Langmuir 1999;15(23):8032–6. https://doi.org/10.1021/la990316o.
[294] Rey M, Fernandez-Rodriguez MA, Karg M, Isa L, Vogel N. Poly-N-Isopropylacrylamide nanogels and microgels at fluid interfaces. Acc Chem Res 2020;53(2):414–24. https://doi.org/10.1021/acs.accounts.9b00528.
[295] Camerin F, Fernández-Rodríguez MÁ, Rovigatti L, Antonopoulou MN, Gnan N, Ninarello A, et al. Microgels adsorbed at liquid-liquid interfaces: a joint numerical and experimental study. ACS Nano 2019;13(4):4548–59. https://doi.org/10.1021/acsnano.9b00390.
[296] Bochenek S, Scotti A, Ogieglo W, Fernández-Rodríguez MÁ, Schulte MF, Gumerov RA, et al. Effect of the 3D swelling of microgels on their 2D phase behavior at the liquid–liquid interface. Langmuir 2019;35(51):16780–92. https://doi.org/10.1021/acs.langmuir.9b02498.
[297] Vialetto J, Nussbaum N, Bergfreund J, Fischer P, Isa L. Influence of the interfacial tension on the microstructural and mechanical properties of microgels at fluid interfaces. J Colloid Interface Sci 2022;608:2584–92. https://doi.org/10.1016/j.jcis.2021.10.186.
[298] Tatry M-C, Laurichesse E, Vermant J, Ravaine V, Schmitt V. Interfacial rheology of model water–air microgels laden interfaces: effect of cross-linking. J Colloid Interface Sci 2023;629:288–99. https://doi.org/10.1016/j.jcis.2022.08.157.
[299] Vasudevan SA, Rauh A, Kröger M, Karg M, Isa L. Dynamics and wetting behavior of Core-Shell soft particles at a fluid-fluid interface. Langmuir 2018;34(50):15370–82. https://doi.org/10.1021/acs.langmuir.8b03048.
[300] Nickel AC, Rudov AA, Potemkin II, Crassous JJ, Richtering W. Interfacial assembly of anisotropic Core-Shell and hollow microgels. Langmuir 2022;38(14):4351–63. https://doi.org/10.1021/acs.langmuir.2c00093.
[301] Bushuev NV, Gumerov RA, Rudov AA, Potemkin II. Compression and ordering of hollow microgels in monolayers formed at liquid-liquid interfaces. Langmuir 2023;39(35):12420–9. https://doi.org/10.1021/acs.langmuir.3c01648.
[302] Vialetto J, Camerin F, Grillo F, Ramakrishna SN, Rovigatti L, Zaccarelli E, et al. Effect of internal architecture on the assembly of soft particles at fluid interfaces. ACS Nano 2021;15(8):13105–17. https://doi.org/10.1021/acsnano.1c02486.
[303] Maldonado-Valderrama J, Del Castillo-Santaella T, Adroher-Benítez I, Moncho-Jordá A, Martín-Molina A. Thermoresponsive microgels at the air-water interface: the impact of the swelling state on interfacial conformation. Soft Matter 2017;13(1):230–8. https://doi.org/10.1039/C6SM01375A.
[304] Schmidt MM, Bochenek S, Gavrilov AA, Potemkin II, Richtering W. Influence of charges on the behavior of polyelectrolyte microgels confined to oil-water interfaces. Langmuir 2020;36(37):11079–93. https://doi.org/10.1021/acs.langmuir.0c02081.
[305] Picard C, Garrigue P, Tatry MC, Lapeyre V, Ravaine S, Schmitt V, et al. Organization of microgels at the air-water interface under compression: role of electrostatics and cross-linking density. Langmuir 2017;33(32):7968–81. https://doi.org/10.1021/acs.langmuir.7b01538.
[306] Tatry MC, Laurichesse E, Perro A, Ravaine V, Schmitt V. Kinetics of spontaneous microgels adsorption and stabilization of emulsions produced using microfluidics. J Colloid Interface Sci 2019;548:1–11. https://doi.org/10.1016/j.jcis.2019.04.020.
[307] Nussbaum N, Bergfreund J, Vialetto J, Isa L, Fischer P. Microgels as globular protein model systems. Colloids Surf B: Biointerfaces 2022;217:112595. https://doi.org/10.1016/j.colsurfb.2022.112595.
[308] Destribats M, Lapeyre V, Sellier E, Leal-Calderon F, Schmitt V, Ravaine V. Water-in-oil emulsions stabilized by water-dispersible poly(N-Isopropylacrylamide) microgels: understanding anti-Finkle behavior. Langmuir 2011;27(23):14096–107. https://doi.org/10.1021/la203476h.
[309] Schmitt C, Moitzi C, Bovay C, Rouvet M, Bovetto L, Donato L, et al. Internal structure and colloidal behaviour of covalent whey protein microgels obtained by heat treatment. Soft Matter 2010;6(19):4876. https://doi.org/10.1039/c0sm00220h.
[310] Stubley SJ, Cayre OJ, Murray BS, Torres IC. Emulsifying properties of sugar beet pectin microgels. Food Hydrocoll 2023;137:108291. https://doi.org/10.1016/j.foodhyd.2022.108291.
[311] Nicolai T. Formation and functionality of self-assembled whey protein microgels. Colloids Surf B: Biointerfaces 2016;137:32–8. https://doi.org/10.1016/j.colsurfb.2015.05.055.
[312] Ishii T, Matsumiya K, Aoshima M, Matsumura Y. Microgelation imparts emulsifying ability to surface-inactive polysaccharides—bottom-up vs top-down approaches. Npj sci. Food 2018;2(1):15. https://doi.org/10.1038/s41538-018-0023-7.
[313] Murray BS. Microgels at fluid-fluid interfaces for food and drinks. Adv Colloid Interf Sci 2019;271:101990. https://doi.org/10.1016/j.cis.2019.101990.
[314] Stigter D. Micelle formation by ionic surfactants. II. Specificity of head groups, micelle structure. J Phys Chem 1974;78(24):2480–5. https://doi.org/10.1021/j100617a013.
[315] Palladino P, Ragone R. Ionic strength effects on the critical micellar concentration of ionic and nonionic surfactants: the binding model. Langmuir 2011;27(23):14065–70. https://doi.org/10.1021/la202897q.
[316] Mukerjee P, Chan CC. Effects of high salt concentrations on the micellization of octyl glucoside: salting-out of monomers and electrolyte effects on the micelle−water interfacial tension 1. Langmuir 2002;18(14):5375–81. https://doi.org/10.1021/la020059e.
[317] Schwierz N, Horinek D, Sivan U, Netz RR. Reversed hofmeister series—the rule rather than the exception. Curr Opin Colloid Interface Sci 2016;23:10–8. https://doi.org/10.1016/j.cocis.2016.04.003.
[318] Yano YF, Kobayashi Y, Ina T, Nitta K, Uruga T. Hofmeister anion effects on protein adsorption at an air–water interface. Langmuir 2016;32(38):9892–8. https://doi.org/10.1021/acs.langmuir.6b02352.
[319] Miyagishi S, Okada K, Asakawa T. Salt effect on critical micelle concentrations of nonionic surfactants, N-acyl-N-Methylglucamides (MEGA-N). J Colloid Interface Sci 2001;238(1):91–5. https://doi.org/10.1006/jcis.2001.7503.
[320] Para G, Jarek E, Warszynski P. The hofmeister series effect in adsorption of cationic surfactants—theoretical description and experimental results. Adv Colloid Interf Sci 2006;122(1–3):39–55. https://doi.org/10.1016/j.cis.2006.06.017.
[321] Ashbaugh HS, Pethica BA. Alkane adsorption at the water−vapor interface. Langmuir 2003;19(18):7638–45. https://doi.org/10.1021/la034559z.

[322] Biscay F, Ghoufi A, Malfreyt P. Adsorption of N-alkane vapours at the water surface. Phys Chem Chem Phys 2011;13(23):11308. https://doi.org/10.1039/c0cp02511a.
[323] Yan W, Zhao G-Y, Chen G-J, Guo T-M. Interfacial tension of (methane + nitrogen) + water and (carbon dioxide + nitrogen) + water systems. J Chem Eng Data 2001;46(6):1544–8. https://doi.org/10.1021/je0101505.
[324] Nielsen LC, Bourg IC, Sposito G. Predicting CO2–water interfacial tension under pressure and temperature conditions of geologic CO2 storage. Geochim Cosmochim Acta 2012;2012(81):28–38. https://doi.org/10.1016/j.gca.2011.12.018.
[325] da Rocha SRP, Johnston KP. Interfacial thermodynamics of surfactants at the CO2 −water interface. Langmuir 2000;16(8):3690–5. https://doi.org/10.1021/la9912601.
[326] King MD, Rennie AR, Thompson KC, Fisher FN, Dong CC, Thomas RK, et al. Oxidation of oleic acid at the air-water interface and its potential effects on cloud critical supersaturations. Phys Chem Chem Phys 2009;11(35):7699–707. https://doi.org/10.1039/b906517b.
[327] Jones SH, King MD, Rennie AR, Ward AD, Campbell RA, Hughes AV. Aqueous radical initiated oxidation of an organic monolayer at the air–water interface as a proxy for thin films on atmospheric aerosol studied with neutron reflectometry. J Phys Chem A 2023;127(42):8922–34. https://doi.org/10.1021/acs.jpca.3c03846.
[328] Tewes F, Boury F. Effect of H2O-CO2 organization on ovalbumin adsorption at the supercritical CO2-water interface. J Phys Chem B 2005;109(5):1874–81. https://doi.org/10.1021/jp046940d.
[329] Vijayendran BR, Bursh TP. Effect of oil phase polarity on the saturation adsorption of sodium lauryl sulfate at oil/water interfaces. J Colloid Interface Sci 1979;68(2):383–6. https://doi.org/10.1016/0021-9797(79)90290-X.
[330] Mędrzycka K, Zwierzykowski W. Adsorption of alkyltrimethylammonium bromides at the various interfaces. J Colloid Interface Sci 2000;230(1):67–72. https://doi.org/10.1006/jcis.2000.7045.
[331] Bergfreund J, Diener M, Geue T, Nussbaum N, Kummer N, Bertsch P, et al. Globular protein assembly and network formation at fluid interfaces: effect of oil. Soft Matter 2021;17(6):1692–700. https://doi.org/10.1039/D0SM01870H.
[332] Murray BS. Equilibrium and dynamic surface pressure-area measurements on protein films at air-water and oil-water interfaces. Colloids Surf A Physicochem Eng Asp 1997;125(1):73–83. https://doi.org/10.1016/S0927-7757(97)00015-0.
[333] Maldonado-Valderrama J, Miller R, Fainerman VB, Wilde PJ, Morris VJ. Effect of gastric conditions on β-Lactoglobulin interfacial networks: influence of the oil phase on protein structure. Langmuir 2010;26(20):15901–8. https://doi.org/10.1021/la102294u.
[334] Maldonado-Valderrama J, Wilde PJ, Mulholland F, Morris VJ. Protein unfolding at fluid interfaces and its effect on proteolysis in the stomach. Soft Matter 2012;8(16):4402–14. https://doi.org/10.1039/c2sm07317j.
[335] Rudin J, Wasan DT. Mechanisms for lowering of interfacial tension in alkali/acidic oil systems: effect of added surfactant. Ind Eng Chem Res 1992;31(8):1899–906. https://doi.org/10.1016/0166-6622(92)80149-V.
[336] Frigerio M, Freire VMR, Soares TA, Amenitsch H, Leser ME, Salentinig S. Interfacial structurization between triolein and water from PH and buffer ions. J Colloid Interface Sci 2024;665:1091–101. https://doi.org/10.1016/j.jcis.2024.03.089.
[337] van Baalen C, Vialetto J, Isa L. Tuning electrostatic interactions of colloidal particles at oil-water interfaces with organic salts. Phys Rev Lett 2023;131(12):128202. https://doi.org/10.1103/PhysRevLett.131.128202.
[338] Bertsch P, Böcker L, Palm A-S, Bergfreund J, Fischer P, Mathys A. Arthrospira platensis protein isolate for stabilization of fluid interfaces: effect of physicochemical conditions and comparison to animal-based proteins. Food Hydrocoll 2023;136:108290. https://doi.org/10.1016/j.foodhyd.2022.108290.
[339] Musen MA, O'Connor MJ, Schultes E, Martínez-Romero M, Hardi J, Graybeal J. Modeling community standards for metadata as templates makes data FAIR. Sci Data 2022;9(1):696. https://doi.org/10.1038/s41597-022-01815-3.
[340] Batista D, Gonzalez-Beltran A, Sansone S-A, Rocca-Serra P. Machine actionable metadata models. Sci Data 2022;9(1):592. https://doi.org/10.1038/s41597-022-01707-6.
[341] Bucher E, Claunch CJ, Hee D, Smith RL, Devlin K, Thompson W, et al. Annot: a Django-based sample, reagent, and experiment metadata tracking system. BMC Bioinform 2019;20(1):542. https://doi.org/10.1186/s12859-019-3147-0.
[342] Jeong J, Park T, Song J, Kang S, Won J, Han J, et al. Integrating data mining and natural language processing to construct a melting point database for organometallic compounds. J Chem Inf Model 2024;64(19):7432–46. https://doi.org/10.1021/acs.jcim.4c01254.
[343] Herrmann D, Hodapp P, Starman M, Huang P-C, Lin C-L, Le LBQ, et al. Enhancing FAIRdata by providing digital workflows from data generation to the publication of data: an open source approach described for cyclic voltammetry. Chem Sci 2025;16(10):4430–41. https://doi.org/10.1039/D4SC08620A.
[344] Masmoudi M, Ben Abdallah Ben Lamine S, Karray MH, Archimede B, Baazaoui Zghal H. Semantic data integration and querying: a survey and challenges. ACM Comput Surv 2024;56(8):1–35. https://doi.org/10.1145/3653317.
[345] Gutierrez C, Sequeda JF. Knowledge graphs. Commun ACM 2021;64(3):96–104. https://doi.org/10.1145/3418294.
[346] Martins DML. Reverse engineering database queries from examples: state-of-the-art, challenges, and research opportunities. Inf Syst 2019;83:89–100. https://doi.org/10.1016/j.is.2019.03.002.
[347] Vita R, Overton JA, Mungall CJ, Sette A, Peters B. FAIR principles and the IEDB: short-term improvements and a long-term vision of OBO-foundry mediated machine-actionable interoperability. Database 2018;2018(2018):1–9. https://doi.org/10.1093/database/bax105.
[348] Abreu-Vicente J, Sonntag H, Eidens T, Mitchell CS, Lemberger T. Integrating curation into scientific publishing to train AI models. Bioinformatics 2026;42(1):1–14. https://doi.org/10.1093/bioinformatics/btaf685.
[349] Wood V, Jeffryes M, Green AF, Blum M, Orchard S, Panni S, et al. Empowering biological knowledgebases: advances in human-in-the-loop AI-driven literature curation. Bioinforma Adv 2026;6(1):vbag028. https://doi.org/10.1093/bioadv/vbag028.
[350] Mondal R, Sen M, Sengupta S, Maity W, Palapetta S, Dhruw NK, et al. Multi-agent AI system for high quality metadata curation at scale. bioRxiv 2025. https://doi.org/10.1101/2025.06.10.658658. 2025.06.10.658658.
[351] Musyaffa FA, Rapp K, Gohlke H. LISTER: semiautomatic metadata extraction from annotated experiment documentation in ELabFTW. J Chem Inf Model 2023;63(20):6224–38. https://doi.org/10.1021/acs.jcim.3c00744.
[352] Andken M, Zheng C, Sun Z, Deutsch EW. Automated metadata extraction from MzML files with RunAssessor. J Proteome Res 2026;25(5):2581–90. https://doi.org/10.1021/acs.jproteome.5c01045.
[353] Lantéri N, Ruhl HA, Gates A, Martínez E, del Rio Fernandez J, Aguzzi J, et al. The EMSO generic instrument module (EGIM): standardized and interoperable instrumentation for ocean observation. Front Mar Sci 2022;9:801033. https://doi.org/10.3389/fmars.2022.801033.
[354] Pieczonka SA, Thomas MJ, Schmitt-Kopplin P, Marshall JW. Harmonization of FT-ICR-MS instruments for interoperable multi-laboratory comprehensive compositional profiling. Anal Chem 2025;97(15):8491–8. https://doi.org/10.1021/acs.analchem.5c00488.
[355] Katritzky AR, Pacureanu LM, Slavov SH, Dobchev DA, Shah DO, Karelson M. QSPR study of the first and second critical micelle concentrations of cationic surfactants. Comput Chem Eng 2009;33(1):321–32. https://doi.org/10.1016/j.compchemeng.2008.09.011.
[356] Astray G, Iglesias-Otero MA, Moldes OA, Mejuto JC. Predicting critical micelle concentration values of non-ionic surfactants by using artificial neural networks. Tenside Surfactant Deterg 2013;50(2):118–24. https://doi.org/10.3139/113.110242.
[357] Boukelkal N, Rahal S, Rebhi R, Hamadache M. QSPR for the prediction of critical micelle concentration of different classes of surfactants using machine learning algorithms. J Mol Graph Model 2024;129:108757. https://doi.org/10.1016/j.jmgm.2024.108757.
[358] Qin S, Jin T, Van Lehn RC, Zavala VM. Predicting critical micelle concentrations for surfactants using graph convolutional neural networks. J Phys Chem B 2021;125(37):10610–20. https://doi.org/10.1021/acs.jpcb.1c05264.
[359] Brozos C, Rittig JG, Bhattacharya S, Akanny E, Kohlmann C, Mitsos A. Predicting the temperature dependence of surfactant CMCs using graph neural networks. J Chem Theory Comput 2024;20(13):5695–707. https://doi.org/10.1021/acs.jctc.4c00314.
[360] Brozos C, Rittig JG, Bhattacharya S, Akanny E, Kohlmann C, Mitsos A. Graph neural networks for surfactant multi-property prediction. Colloids Surfaces A Physicochem Eng Asp 2024;694:134133. https://doi.org/10.1016/j.colsurfa.2024.134133.
[361] Brozos C, Rittig JG, Akanny E, Bhattacharya S, Kohlmann C, Mitsos A. Predicting the temperature-dependent CMC of surfactant mixtures with graph neural networks. Comput Chem Eng 2025;198:109085. https://doi.org/10.1016/j.compchemeng.2025.109085.
[362] Fan F, Yu H, Huang Y, Li X, Fu X. Study on the adsorption performance of ionic liquids based on molecular dynamics and interpretable machine learning. J Chem Inf Model 2025;65(22):12305–12. https://doi.org/10.1021/acs.jcim.5c01402.
[363] Vermeire FH, Chung Y, Green WH. Predicting solubility limits of organic solutes for a wide range of solvents and temperatures. J Am Chem Soc 2022;144(24):10785–97. https://doi.org/10.1021/jacs.2c01768.
[364] Sridharan S, Ettelaie R, Sarkar R, Afzali M, Dela H, Murray BS, et al. Data-driven pipeline enables discovery of plant protein surfactants. ChemRxiv 2026. https://doi.org/10.26434/chemrxiv.15000208/v1.
[365] Gelman S, Johnson B, Freschlin CR, Sharma A, D'Costa S, Peters J, et al. Biophysics-based protein language models for protein engineering. Nat Methods 2025;22(9):1868–79. https://doi.org/10.1038/s41592-025-02776-2.
[366] Attia L, Burns JW, Doyle PS, Green WH. Data-driven organic solubility prediction at the limit of aleatoric uncertainty. Nat Commun 2025;16(1):7497. https://doi.org/10.1038/s41467-025-62717-7.
[367] Moura SR, Furtado A, Pellegrino O, Lenard E, Malejczyk E, Sariyerli G, et al. Surface tension measurements – a comparative study. Acta IMEKO 2023;12(4):1–6. https://doi.org/10.21014/actaimeko.v12i4.1418.
[368] Eastman P, Behara PK, Dotson DL, Galvelis R, Herr JE, Horton JT, et al. SPICE, a dataset of drug-like molecules and peptides for training machine learning potentials. Sci Data 2023;10(1):11. https://doi.org/10.1038/s41597-022-01882-6.
[369] Xerxa E, Vogt M, Bajorath J. Influence of data curation and confidence levels on compound predictions using machine learning models. J Chem Inf Model 2024;64(24):9341–9. https://doi.org/10.1021/acs.jcim.4c01573.
[370] McMurry JA, Juty N, Blomberg N, Burdett T, Conlin T, Conte N, et al. Identifiers for the 21st century: how to design, provision, and reuse persistent identifiers to maximize utility and impact of life science data. PLoS Biol 2017;15(6):e2001414. https://doi.org/10.1371/journal.pbio.2001414.
[371] Petković D. JSON integration in relational database systems. Int J Comput Appl 2017;168(5):14–9. https://doi.org/10.5120/ijca2017914389.
[372] Lv T, Yan P, He W. Survey on JSON data modelling. J Phys Conf Ser 2018;1069(1):012101. https://doi.org/10.1088/1742-6596/1069/1/012101.

[373] Yap CW. PaDEL-descriptor: an open source software to calculate molecular descriptors and fingerprints. J Comput Chem 2011;32(7):1466–74. https://doi.org/10.1002/jcc.21707.
[374] Moriwaki H, Tian Y-S, Kawashita N, Takagi T. Mordred: A molecular descriptor calculator. J Cheminform 2018;10(1):4. https://doi.org/10.1186/s13321-018-0258-y.
[375] Wang L, Ding J, Pan L, Cao D, Jiang H, Ding X. Quantum chemical descriptors in quantitative structure–activity relationship models and their applications. Chemom Intell Lab Syst 2021;217(June):104384. https://doi.org/10.1016/j.chemolab.2021.104384.